Wang *et al. Chem Synth* 2023;3:8
DOI: 10.20517/cs.2022.34

Chemical Synthesis

Review

Open Access

Recent advances in nonmetallic modulation of palladium-based electrocatalysts

Caikang Wang[1,2], Xian Jiang[1,*], Yufei Wang[3], Yawen Tang[3], Juan Zhou[2,*], Gengtao Fu[3,*]

[1]School of New Energy, Nanjing University of Science and Technology, Jiangyin 214443, Jiangsu, China.
[2]School of Energy and Power Engineering, Nanjing University of Science and Technology, Nanjing 210094, Jiangsu, China.
[3]Jiangsu Key Laboratory of New Power Batteries, Jiangsu Collaborative Innovation Center of Biomedical Functional Materials, School of Chemistry and Materials Science, Nanjing Normal University, Nanjing 210023, Jiangsu, China.

[*]**Correspondence to:** Dr. Xian Jiang, School of New Energy, Nanjing University of Science and Technology, No. 8 Fuxing Road, Jiangyin 214443, Jiangsu, China. E-mail: xianjiang@njust.edu.cn; Prof. Juan Zhou, School of Energy and Power Engineering, Nanjing University of Science and Technology, No. 200 Xiaolingwei Street, Nanjing 210094, Jiangsu, China. E-mail: jzhou@njust.edu.cn; Prof. Gengtao Fu, Jiangsu Key Laboratory of New Power Batteries, Jiangsu Collaborative Innovation Center of Biomedical Functional Materials, School of Chemistry and Materials Science, Nanjing Normal University, No.1 Wenyuan Road, Nanjing 210023, Jiangsu, China. E-mail: gengtaofu@njnu.edu.cn

How to cite this article: Wang C, Jiang X, Wang Y, Tang Y, Zhou J, Fu G. Recent advances in nonmetallic modulation of palladium-based electrocatalysts. *Chem Synth* 2023;3:8. https://dx.doi.org/10.20517/cs.2022.34

Received: 30 Oct 2022 **First Decision:** 2 Dec 2022 **Revised:** 15 Jan 2023 **Accepted:** 1 Feb 2023 **Published:** 15 Feb 2023

Academic Editors: Bao-Lian Su, Xiangdong Yao **Copy Editor:** Ke-Cui Yang **Production Editor:** Ke-Cui Yang

Abstract

Modulating the electrocatalytic performance of Palladium (Pd) with nonmetallic elements (e.g., H, B, C, N, O, P and S) has gained ever-increasing attention since their introduction has been proven to effectively modulate the 3d-electronic configuration and subsurface properties of Pd. In this review, the most advanced nonmetal-modified Pd-based catalysts are classified according to the different doped atoms (i.e., hydrides, borides, carbides, nitrides, oxides, phosphides and sulfides) and critically reviewed to emphasize the roles of nonmetallic elements doping on various electrocatalytic reactions. In each section, the synthetic strategies developed to incorporate nonmetals are discussed in detail. Furthermore, the optimized approaches of nonmetals-doped Pd-based catalysts and corresponding electrocatalytic enhancement mechanisms are also discussed clearly. Finally, the current challenges and future perspectives regarding nonmetal-modified Pd-based nanocatalysts are also outlined.

Keywords: Pd-based catalysts, nonmetallic modulation, alloy, electronic structure, electrocatalysis

INTRODUCTION

With the persistent traditional fossil fuel consumption and concomitant environmental crisis, it has been an urgent demand for the rapid development of renewable and sustainable energy storage/conversation systems[1,2]. Electrocatalysis is the crucial component of clean energy conversion and technology for achieving the global mission of "carbon neutrality"[3-5]. Exploring high-performance electrocatalysts to promote the sluggish reaction kinetics of electrocatalytic reactions is quite essential. In comparison to the non-noble metal catalysts, Pt-based noble metals are still the state-of-the-art and most extensively used catalysts in the field of electrocatalysis as a result of their attractive catalytic performance and corrosion resistance, but their large-scale commercialization is greatly impeded to the scarce reservation and fancy price[6-9]. Thus, seeking non-Pt-based noble metals as an effective alternative has become urgently needed[10]. Pd, as one of the Pt group metals, with more bountiful reserves (2 to 3 times), similar electronic structure, and close catalytic performance of Pt, has been regarded as a significant research object[11,12]. However, the performance of Pd is still far from satisfactory compared with Pt, which can be attributed to the inferior oxygen and electrochemical dissolubility resistance under high potentials and harsh acidic/alkaline catalytic conditions[13,14].

In recent years, considerable efforts have been made to trim down the cost along with maximum utilization of Pd-based materials by a bunch of optimized strategies, such as heterogeneous interface designing, supporting engineering, strain engineering, crystal phase engineering, microstructure regulation, and heteroatom doping[14-18]. These strategies can efficiently modulate the catalytic property of Pd-based materials and thus provide ways to generate efficient and stable nanocatalysts. Among the proposed strategies, the metal and/or nonmetallic heteroatoms doping in Pd lattice to form alloy/intermetallic nanocatalysts have been extensively investigated as one of the most effective approaches to overcome the obstacle of poor stability, high costs, and scarcity[19,20]. Especially, the introduction of the nonmetallic heteroatoms (e.g., H, B, C, N, O, P and S) can regulate the structural and electronic properties of Pd, thus effectively modulating the overall work function and engineering the surface adsorption at active sites, ultimately leading to enhanced electrocatalytic activity and stability. The rising of nonmetal-modulated strategies enriches the research system of Pt-free electrocatalysts while promoting research progress in Pd-based electrocatalysts. With increased focus on energy-related catalysis in the past few years, a number of nonmetal-implanted Pd-based electrocatalysts have been identified to be promising for many electrocatalytic reactions, such as oxygen reduction/evolution reactions (ORR/OER), hydrogen evolution/oxidation reactions (HER/HOR), N_2 reduction reaction (NRR), CO_2 reduction reaction (CO_2RR), alcohol oxidation reaction (AOR), and formic acid oxidation reaction (FAOR), *etc.*[21-24] Although some reviews on nonmetal-doped noble metals have been reported, there are still limitations. *Chen et al.* introduce the development of nonmetals-doped precious metals, but to some extent, it occupies the space for a detailed understanding of nonmetal-doped Pd-based catalysts[25]. Other targeted reviews on nonmetal-doped Pd-based catalysts did not discuss all common nonmetals (e.g., H, B, C, N, O, P, and S)[26,27].

In this review, the most advanced nonmetals-doped Pd-based catalysts were classified on the basis of the different doped atoms to be hydrides, borides, carbides, nitrides, oxides, phosphides, and sulfides [Figure 1]. We focus on the development of the nonmetallic atoms doped Pd-based nanocrystals with diverse compositions, stoichiometries, morphologies, and their resulting performance as catalysts for almost all mainstream electrocatalytic reactions. In each section, we will introduce the enhancement mechanisms in detail. Notably, the optimized strategies of nonmetals-doped Pd-based catalysts and the corresponding electrocatalytic applications were discussed together to reveal the effectiveness of the improved approaches more clearly. Finally, the challenges and outlooks for future nonmetal-doped Pd-based electrocatalysts are proposed.

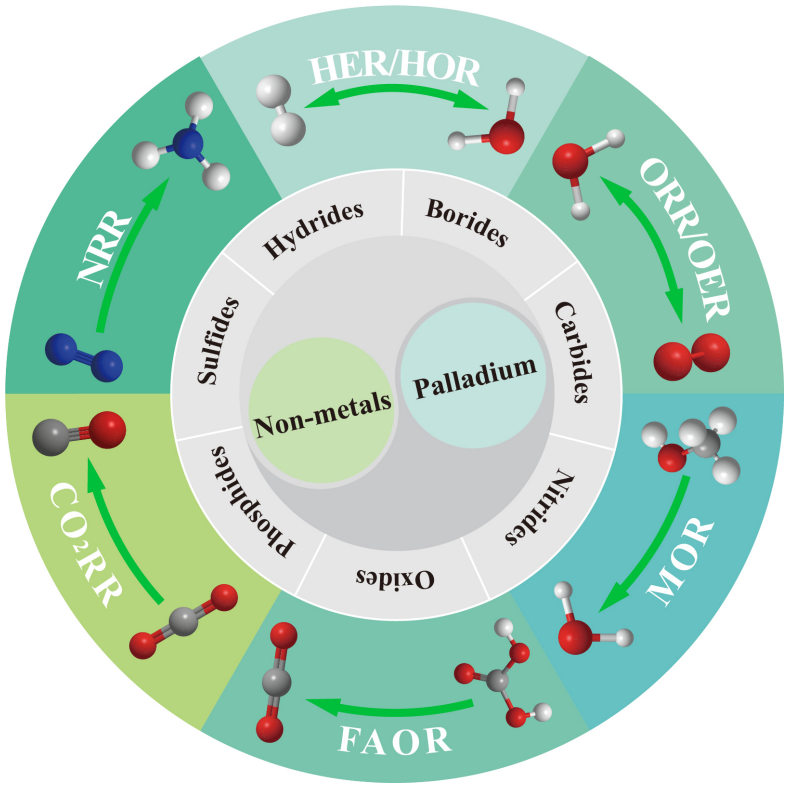

Figure 1. Schematic illustration of nonmetal-doped Pd-based catalysts towards electrocatalytic applications.

ADVANTAGES OF NONMETAL-DOPING

The merits of doping nonmetals into the Pd lattice have made it an attractive choice to modify the crystal and electronic structure of Pd. For one thing, the doping of nonmetal atoms into Pd can be classified into interstitial and substitutional doping. Theoretically, those nonmetal atoms (e.g., H, B, C, N) with small atomic radii tend to incorporate into interstitial sites within Pd lattices rather than substitute Pd atoms, while other nonmetals (e.g., O, P, S) with a relatively large radius can either occupy the interstitial lattice sites of the Pd lattice or substitute Pd atoms. The difference in atomic radius can induce the Pd lattice strain effect and abundant structural defects. Moreover, Pd-nonmetal alloys possess a rich phase compared to Pd-metal alloys. Pd with the face-centered cubic structure will also form other crystal phases or amorphous structures after B, P, or S doping, and the modified Pd crystal phase evolution offers more opportunities to optimize the catalytic properties. For another, the apparent electronegativity difference between Pd and nonmetal atoms can also arouse the significant charge transfer between Pd and adjacent nonmetallic atoms, thus effectively optimizing the electronic structure of Pd sites. Meanwhile, unlike the *d*-*d* orbital coupling between Pd and transition metals, the *s*, *p*-orbitals of nonmetallic heterometals would coordinate with the *d*-orbital of Pd atoms to form the *s*, *p*-*d*-conjugated structure, resulting in the improved electronic structure and *d*-band center of Pd sites. This optimized electronic structure is believed to modulate the reaction intermediates' adsorption energy and lower the activation energy of the chemical reactions, thus ultimately improving their catalytic performance. Finally, nonmetals with abundant resources, easy availability and low cost provide effective ways for the cost reduction of Pd-based electrocatalysts.

SYNTHESIS AND ELECTROCATALYTIC APPLICATIONS

H-doped Pd-based nanocrystals

Tremendous attention has been focused on the hydrogen (H) atoms dopant into Pd-based catalysts compared with other nonmetallic elements due to the smallest atomic radius of H among all atoms and favorable affinity towards Pd. This advantage makes H atoms easier to penetrate into the interstitial sites within the Pd lattice structure, and thermodynamic equilibrium can be obtained in a short time by an extremely high migration rate in the parent metal, resulting in the final formation of Pd-based hydrides and an expanded Pd lattice spacing[28]. Essentially, the changed lattice parameters of Pd and subsequently altered charge transfer between the host and guest metals would generate available electron structures for Pd-based catalysts for improved electrocatalytic activity and selectivity[29]. Inspired by this point, the control synthesis of palladium hydride (PdH_x) nanocatalysts via incorporating H atoms into the space lattice of Pd would be expected to be a fascinating route for addressing the relatively poor catalytic performances of pure Pd catalysts.

General speaking, the synthetic routes of the Pd-based hydrides could be briefly summarized as the direct exposure of Pd-based nanocrystals in the H_2-containing atmosphere under certain conditions, mainly including (i) traditional gaseous H_2 treatment[30,31], the prefabricated Pd nanocrystals were transferred into H_2 atmosphere at a certain condition; (ii) post hydrogenation treatment[32-34], the prefabricated Pd-based nanocrystals were hydrogenated with H_2 generated from the decomposition of the solvents (e.g., DMF[35], $NaBH_4$[36], N_2H_4[37], HCHO[38], amine molecules[39,40], and alcohol molecules[41]); (iii) in-situ hydrogenation treatment, direct hydrogenation during preparation[29,42-44]. Typically, the hydrogenated steps include gaseous hydrogen adsorbing on the surface of Pd-based nanocrystals, penetrating the Pd phase, and then occupying the interstitial sites of the Pd lattice. Moreover, another method to prepare PdH_x is applying a negative potential to drive the evolved H atoms into the lattice of Pd nanocrystals. To better understand the roles of different H sources, examples of common H sources and their electrocatalytic performances are summarized in Table 1.

In theory, the electrocatalytic property of Pd-based electrocatalysts could be optimized via two effective ways: (i) electronic regulation to promote the intrinsic activity of each active site via interface engineering and controlling the crystal plane structure, electronic effect and stress effect of the catalysts; (ii) structural regulation to increase the number of surficial active sites via enlarging the specific surface area, increasing the defect sites and introducing carriers. It has been a paradigm for a long that efficiently tuning Pd-based electrocatalyst activity and durability through electronic and structural regulation. In fact, the hydrogenation of Pd-based catalysts usually requires a high-pressure condition, which often accompanies H atoms to gradually leach out over time, even at room temperature[55,56]. More terribly, the as-prepared PdH_x nanocatalysts have worse stability due to the spontaneous release of hydrogen under ambient conditions. Earlier studies have proved that amorphous materials are a kind of metastable materials with the absence of defects, which have displayed superior corrosion resistance and catalytic properties[57,58]. Amorphous materials can be used as a protective shell to significantly enhance the stability of as-prepared PdH_x nanocatalysts. Typically, Liu *et al.*[31] proposed a novel strategy that incorporated amorphous CuO with PdH_x nanocubes treated with the gas H_2 to cope with the unsatisfactory hydrogen stability. The external layer of dense amorphous CuO has a certain ability to isolate hydrogen ions, resulting in preventing H atoms from escaping. With the introduction of amorphous CuO, the $PdH_{0.43}$@CuO nanocubes show excellent long-term stability. This strategy of enhancing stability can also be extended to other synthetic methods. One notable example is given by Lu *et al.*, who used simple DMF treatment of Pd nanocubes in combination with two-dimensional amorphous NiB nanosheets via the $NaBH_4$ reduction of Ni species to form $PdH_{0.706}$@NiB composites, resulting in a highly efficient and durable ORR electrocatalyst[45]. The improved ORR activity and stability both arise from the strong interaction between $PdH_{0.706}$ nanocubes and

Table 1. List of common H sources and electrocatalytic applications of Pd-based hydrides.

Catalysts	H source	Synthetic route	Electrolyte	Performance	Ref.
ORR					
$PdH_{0.33}$ NDs	OAm	*In-situ* hydrogenation treatment	0.1 M KOH	$E_{1/2}$ = 0.91 V; MA = 0.72 A mg^{-1} at 0.9 V; SA = 1.25 mA cm^{-2} at 0.9 V	[29]
$PdH_{0.43}$ @CuO NCs	H_2	Gaseous H_2 treatment	0.1 M KOH	$E_{1/2}$ = 0.89 V; MA = 0.18 A mg^{-1} at 0.9 V	[31]
$PdH_{0.706}$ NCs	DMF	Post hydrogenation treatment	0.1 M $HClO_4$	$E_{1/2}$ = 0.89 V; MA = 0.75 A mg^{-1} at 0.9 V; ECSA = 50 m^2 g^{-1}	[45]
$PdH_{0.706}$@Ni-B NCs	DMF	Post hydrogenation treatment	0.1 M $HClO_4$	$E_{1/2}$ = 0.91 V; MA = 1.05 A mg^{-1} at 0.9 V; ECSA = 52 m^2 g^{-1}	[45]
$PdH_{0.64}$ icosahedra	DMF	Post hydrogenation treatment	0.1 M KOH	$E_{1/2}$ = 0.91 V; MA = 0.55 A mg^{-1} at 0.9 V	[46]
HER					
RhPdH NPs	CH_3CHO	*In-situ* hydrogenation treatment	1 M KOH	η_{10} = 36.6 mV; Tafel slope = 35.3 mA dec^{-1}; TOF = 0.33 s^{-1}	[47]
RhPdH NSs	HCHO	*In-situ* hydrogenation treatment	1 M KOH	η_{10} = 40 mV; Tafel slope = 35.7 mA dec^{-1}	[42]
IrPdH NDs	C_2H_5OH	Post hydrogenation treatment	0.5 M H_2SO_4 1 M KOH 1 M PBS	acidic: η_{10} = 14 mV; Tafel slope = 35.21 mA dec^{-1}; TOF = 0.26 s^{-1} alkaline: η_{10} = 25 mV; Tafel slope = 47 mA dec^{-1}; TOF = 0.14 s^{-1}. neutral: η_{10} = 60 mV; Tafel slope = 47 mA dec^{-1}; TOF = 0.035 s^{-1}	[41]
PdH-NDs	DMF	Post hydrogenation treatment	1 M KOH	η_{10} = 358 mV; Tafel slope = 130 mA dec^{-1}	[48]
$PdCu_{0.2}H_{0.43}$ /C	OAm	Post hydrogenation treatment	1 M KOH	η_{10} = 28 mV; Tafel slope = 23 mA dec^{-1}	[49]
MOR					
$PdH_{0.43}$@Pt NPs	DMF	Post hydrogenation treatment	1 M KOH + 1 M CH_3OH	MA = 3.68 A mg_{Pd+Pt}^{-1}; ECSA = 15.11 m^2 g^{-1}	[35]
$PdH_{0.43}$ NDs	n-butylamine	*In-situ* hydrogenation treatment	1 M KOH + 1 M CH_3OH	MA = 2.18 A mg^{-1}; TOF = 0.76 s^{-1}	[43]
$PdH_{0.43}$ NCs	DMF	Post hydrogenation treatment	0.1 M KOH + 0.1M CH_3OH	SA = 1.23 mA cm^{-2}	[50]
$PdH_{0.43}$ NCs	DMF	Post hydrogenation treatment	1 M KOH + 1 M CH_3OH	MA = 0.92 A mg^{-1}; SA = 58.2 mA cm^{-2}	[51]
PdMoH NSs	OAm	*In-situ* hydrogenation treatment	1 M KOH + 1 M CH_3OH	MA = 3.56 A mg^{-1}; SA = 6.06 mA cm^{-2}	[44]
FAOR					
$PdH_{0.43}$ NDs	DMF	Post hydrogenation treatment	0.1 M KOH + 0.5 M HCOOH	MA = 0.85 A mg^{-1}; ECSA = 16.4 m2 g^{-1}	[48]
ß-PdH NCs	DMF	Post hydrogenation treatment	0.5 M $HClO_4$ + 0.5 M HCOOH	MA = 4.40 A mg^{-1}; SA = 7.48 mA cm^{-2}	[52]
$PdH_{0.43}$ NCs	n-butylamine	Post hydrogenation treatment	0.5 M H_2SO_4 + 0.25 M HCOOH	MA = 1.04 A mg-1; SA = 6.82 mA cm^{-2}	[40]
$PdH_{0.43}$ NCs	n-butylamine	Post hydrogenation treatment	0.5 M H_2SO_4 + 0.25 M HCOOH	MA = 1.06 A mg^{-1}; SA = 5.11 mA cm^{-2}	[53]
$PdH_{0.706}$ NCs	N_2H_4	*In-situ* hydrogenation treatment	0.5 M $HClO_4$ + 0.5 M HCOOH	MA = 5.40 A mg^{-1}	[37]
NRR					
$PdH_{0.43}$ NCs	DMF	Post hydrogenation treatment	0.1 M Na_2SO_4	NH_3 yield = 20.4 μg h^{-1} mg^{-1} cat.; FE_{NH3} = 43.6% at -0.15 V; ECSA = 39 m^2 g^{-1}	[32]
$PdH_{0.43}$ NRs	DMF	Post hydrogenation treatment	0.1 M Na_2SO_4	NH_3 yield = 17.53 μg h^{-1} mg^{-1} cat.; FE_{NH3} = 18.56% at -0.15 V; ECSA = 62.1 m^2 g^{-1}	[34]
CO_2RR					

TiO_2-$PdH_{0.43}$ NCs	DMF	Post hydrogenation treatment	0.1 M Na_2SO_4	FE_{CH4} = 82% at -0.6 V	[33]
$PdH_{0.40}$ NCs	DMF	Post hydrogenation treatment	0.1 M $KHCO_3$	FE_{CO} = ~59% and FE_{H2} = ~36% at -0.6 V	[54]

ECSA: electrochemcial active surface area; FE: faradic efficiency; MA: mass activity; NRs: nanorods; NCs: nanocubes; NDs: nanodendrites; NTs: nanotetrahedrons; SA: specific activity; TOF: turnover frequency; η_{10}: overpotentials at 10 mA cm^{-2}. Note that: All potentials are relative to the RHE when without other annotations.

NiB nanosheets. Such interaction induced by the electron-deficient BO^{2-} species in the amorphous NiB membrane can effectively tune the binding energies of O and OH species. These studies illustrate the importance of introducing amorphous materials and provide new opportunities for designing superior stability and activity of Pd-based hydrides.

Apart from the introduction of amorphous materials to form the core-shell structure, the electrocatalytic performance of Pd-based hydrides could also be activated by another composition regulation way of forming the PdM alloy hydrides. Recently, Pd-based bimetallic hydrides (PdMH) have attracted increasing attention in the field of electrocatalysis. This novel approach for enhancing performance is to modify PdH_x catalysts with transition metal (M), such as Ir[41], Rh[42,47], Mo[44], Ni[43], Pt[35], *etc.* In the case of PdMH, the introduction of the secondary metal can not only increase the utilization of Pd atoms, but also enhance the stability and electroactivity due to the combined effects of ligand effect, geometric effect and alloy effect. For example, Cui *et al.* have provided useful insights into the design and synthesis of PdMH catalysts and the corresponding structure-activity relationship. They proposed a facile synthesis of RhPdH with different structures via a one-pot solvothermal method through simultaneous reduction of palladium(II) acetylacetonate [$Pd(acac)_2$] and ruthenium(III) acetylacetonate [$Rh(acac)_3$] with aldehydes as H source, to successfully achieve the alloy hydrides with high activity and robust stability[42,47]. They found that the stable alloy hydrides can only be obtained through the combination of H atoms and alloy structures [Figure 2A]. On the one hand, doping H atoms into RhPd alloy will increase the electronic density, enlarge the bond distance and lower the coordination number of Pd and Rh, induced by the electronic interaction between Rh/Pd 4*d* and H 1*s* states (ligand effect), which is consistent with the situation observed in the Pd-H system[50,53,59]. On the other hand, the added Rh substantially can enhance the binding of H in the alloy [Figure 2B], indicating the RhPdH possess a very large formation enthalpy (alloy effect), corresponding to a very stable hydride. In another work of their group, authors further revealed that the incorporation of H atoms could cause the large lattice expansion of Pd and strong Pd-H orbital hybridization via combining physical characterizations and theoretical results. As demonstrated by the high-resolution X-ray photoelectron spectroscopy (XPS) spectra in Figure 2C, the electronic interaction between Pd and H is stronger than that between Rh and H in the RhPd-H system due to the more positive peak shift (0.67 eV > 0.30 eV), indicating more electron transfer occurs on the Pd atoms. Moreover, the higher intensity of the first near-edge peaks of RhPd-H NPs than that in the RhPd NPs in the extended X-ray adsorption fine structure (EXAFS) experiment also indicated the *s, p-d* orbital hybridization in RhPd-H NPs [Figure 2D], consistent with the XPS results. Notably, the interstitial C incorporation could also induce the expansion of crystal lattice, which would hinder the real understanding of Pd lattice expansion. Fourier transform infrared (FTIR) spectra unambiguously identified that the Pd lattice expansion was actually induced by the doping interstitial H atoms since the FTIR peaks of the simulated H interstitially modified RhPd NPs match well with those of the as-fabricated RhPd-H NPs [Figure 2E]. The large lattice expansion and strong Pd-H orbital hybridization would achieve a longer bond distance and smaller coordination number in RhPd-H system, which is verified by the FT-EXAFS spectra of the Pd K-edge [Figure 2F]. From the viewpoint of reaction kinetics, these results contribute to the weakened hydrogen adsorption on Pd and Rh sites and the optimized HER activities. Indeed, the enhancement mechanism in the RhPd-H system is also applied in

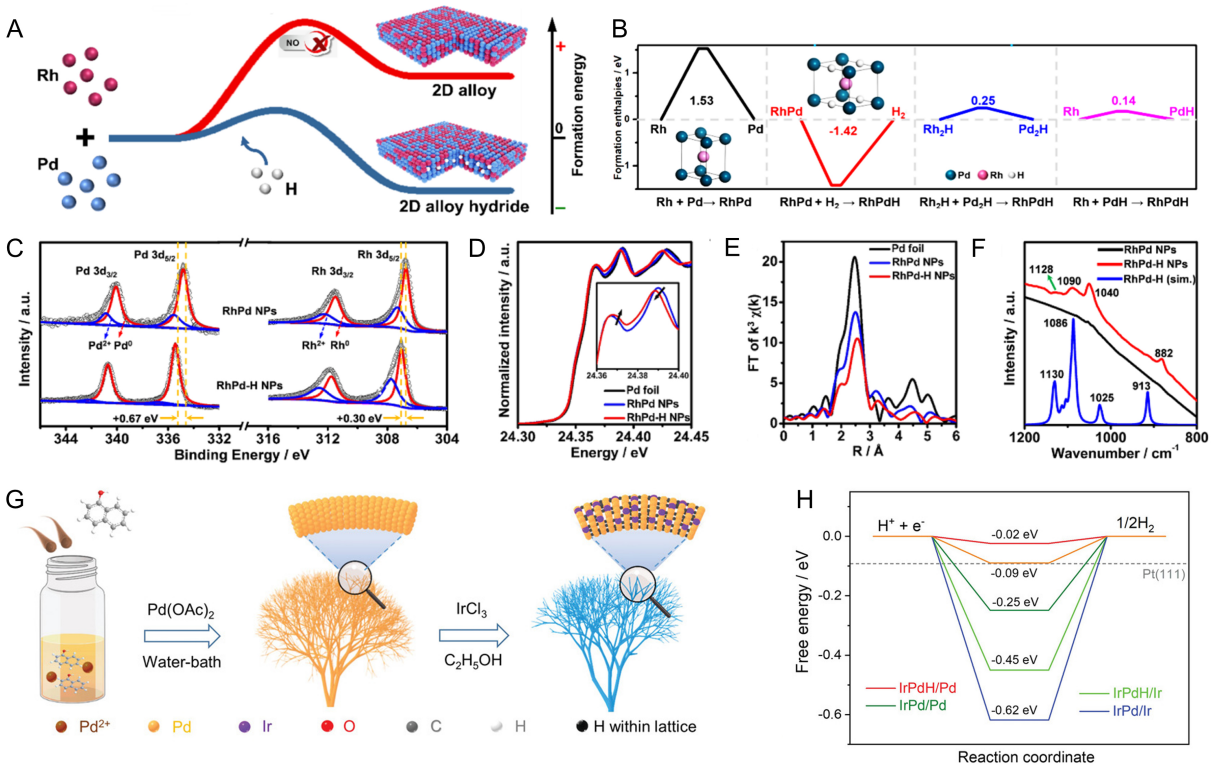

Figure 2. Design of PdMH nanocatalysts with different structures and reaction properties. (A) Different formation energy diagram of 2D RhPd and RhPdH alloy nanosheet; (B) formation enthalpies diagram of different ground-state RhPdH. (A and B) reproduced with permission from[42]: Copyright 2022, American Chemical Society; (C) Pd and Rh 3d spectra of the RhPd-H NPs and RhPd NPs; (D) EXAFS spectra of the Pd K-edge; (E) FTIR spectra of the RhPd NPs, the RhPd-H NPs, and the simulated RhPd-H NPs, respectively; (F) FT-EXAFS spectra of the Pd K-edge; (C-F) reproduced with permission from[47]: Copyright 2019, American Chemical Society; (G) schematic illustration of the synthesis of the IrPdH nanodendrites; (H) diagram of the HER free energy on IrPdH and its counterparts; (G and H) reproduced with permission from[41]: Copyright 2022, Wiley-VCH.

other PdMH nanostructures. More recently, our group also reported an ethanol-induced two-step solvothermal synthesis strategy to prepare IrPdH nanodendrites, which exhibit superior HER activity and stability in the whole pH range [Figure 2G][41]. The hydrogenation mechanism of Pd-based hydrides was sufficiently investigated and discussed, in which the H atoms were produced from the -OH and -CH_2- groups in the ethanol solvent, facilitating the formation of IrPdH. After the insertion of H/Ir atoms, the adsorption Gibbs free energy of *H could be effectively regulated via shifting the *d*-band center relative to the Fermi level, thus promoting the hydrogen formation process, which is verified by a series of density functional theory (DFT) calculations [Figure 2H]. Moreover, the ultrafine dendrite and three-dimensional porous structure can endow the IrPdH catalyst with plentiful accessible active sites and rapid channels for mass/electron transfer and diffusion, contributing to excellent HER activity. This work unambiguously uncovers that the formation of PdMH provides considerable potential for the design of active and stable electrocatalysts. It is worth pointing out that the above-mentioned PdMH nanocatalysts with different nanostructures were endowed with more accessible active sites and large surface reaction areas (geometric effect), demonstrating that nanostructure engineering also imparts a significant contribution in boosting electrocatalytic activity and stability.

Controlled facets of nanocatalysts are another typical way to activate the electrocatalytic performance of Pd-based hydrides, and it has attracted remarkable attention because of the correlation between surface properties and catalytic activity[60-62]. Typically, in terms of structure control, the surface atomic

arrangement, namely the facet, is believed to be important for improving the electrocatalytic performance, mainly due to the electrocatalytic reaction are highly structure-sensitive and involve both the surface adsorption/desorption and interface catalytic process[63]. Indeed, combining specific facets with interstitial H atom doping has been demonstrated to facilitate catalytic activity and stability[38,52]. Therefore, in the past decades, intensive studies have been carried out on constructing Pd-based hydrides with various exposed crystal facets and exploring the relationship between exposed facets and electrocatalytic activity.

An exciting fact was found that the Pd single crystals followed an active trend of Pd{110} < Pd{111} < Pd{100} in an acid solution when served as ORR catalysts, which was reported by Hoshi *et al*[64]. Moreover, in other work by Erikson *et al.*, it was found that the Pd{100} nanocubes exhibited lower OH_{ad} coverage than that of Pd{110}, which facilitated the increase in its reaction sites toward ORR[65,66]. Given the important role of Pd-based hydrides, these studies not only deepen the fundamental understanding of facet engineering to enhance the electrocatalytic activity but also offer a promising strategy for designing high-performance Pd-based hydrides with specific active facets. For example, Zhang *et al.* prepared three types of $PdH_{0.43}$ nanocrystals (cubic, octahedral and rhombic dodecahedral) with different surface structures enclosed by {100}, {111}, {110} facets, respectively, *via* a facial *n*-butylamine treatment of prefabricated Pd nanocrystals[40]. The three as-prepared $PdH_{0.43}$ nanocrystals served as highly efficient catalysts for FAOR with the activity and stability order as $PdH_{0.43}${100} > $PdH_{0.43}${111} > $PdH_{0.43}${110}. Regarding the catalytic mechanism, the authors also attributed the enhanced catalytic performance to the distinct electronic structure of PdH_x. Due to the different electronegativity between Pd and H atoms, the interstitial H doping would cause the electronic transfer between Pd and H, which lead to the downshift of the Pd *d*-band center[45,48,53,67]. This *d*-band shift results from the interaction of H with Pd, known as the "ligand effect"[68,69], which can weaken the binding strength between reaction intermediates and the catalyst surface. Hence, benefiting from the synergies of facets control and ligand effect, the $PdH_{0.43}${100} exhibits the highest catalytic activity and stability. Similarly, Bu *et al.* also highlighted the benefits of the synergies effect of Pd-based hydrides for the electrocatalysis enhancement[46]. They successfully created Pd–H icosahedra/C with twinned {111} facet by a wet-chemical approach and investigated their electronic behaviors and active origin in ORR by DFT. The authors explained that the enhanced ORR performance is not only attributed to the optimized electronic structure induced by the ligand effect, but more importantly, the twined {111} facet in Pd-H icosahedra/C can further minimize the ORR barrier and adjust the binding strength of key intermediates involved in dissociative mechanisms on the surface of Pd–H (111)-twin, including 2*O, *O + *OH, *O, and *OH [Figure 3A]. When constructing the twin-crystal Pd-H {111} surface, the overpotential can be further reduced from 0.60 V to 0.43 V owing to the combined effects between the close-packed structure and introduced H [Figure 3B]. In addition, the twin-crystal Pd-H {111} surface holds a moderate OH binding strength nearly occupied the peak of $4e^-$ activity volcano map as well as moderate density of state [Figure 3C and D], indicating the twined {111} faceted Pd–H icosahedra/C has the best electrocatalytic activity toward ORR, as evidenced by the polarization curves. The Pd-H icosahedra/C exhibits the most positive half-wave potential of 0.91 V *vs.* RHE among these four catalysts in 0.1 M KOH [Figure 3E].

According to the above discussion, it is strongly verified that the synergistic merits of facets control and ligand effect are helpful for improving the electrocatalytic performance of Pd-based hydrides. To better illustrate the catalytic mechanism of facet-controlled and H-doped Pd, a relatively complete picture of enhancing catalytic performance in Pd-H systems is presented based on recent reports[48,52-54]: (i) in the hydrogeneration process for Pd, the H atoms occupy the octahedral interstitial sites of Pd lattice, and then produce an isotropic lattice expansion induced by different atomic radii. As a result, The surface lattice strain or possible defects might be introduced, leading to the improved surface and catalytic properties of

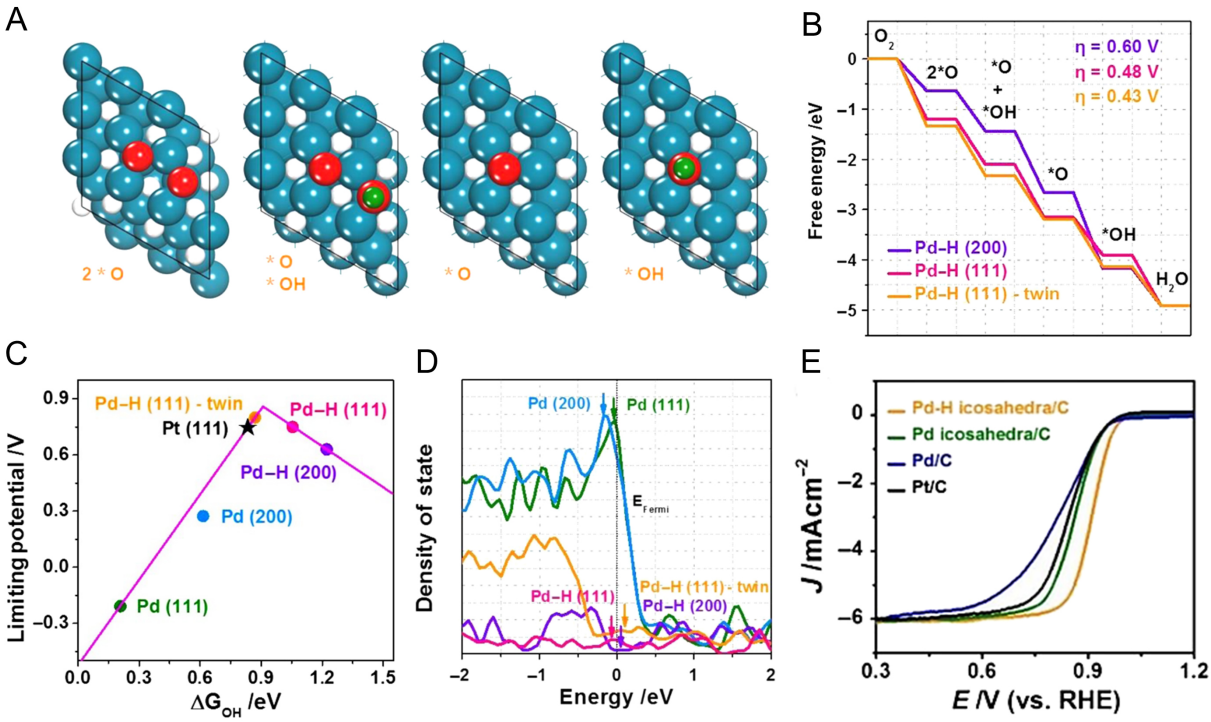

Figure 3. Facet effect applied in Pd-based hydrides. (A) The structural model of intermediates; (B) diagram of ORR process energy profile on different Pd-H surfaces; (C) diagram of the optimized OH binding of twin-crystal Pd-H {111} surface (D) diagram of the moderate density of state on twin-crystal Pd-H {111} surface; (E) ORR polarization curves of various catalysts in 0.1 M KOH; (A-E) reproduced with permission from[46]: Copyright 2021, Chinese Chemical Society.

the PdH_x catalysts; (ii) due to the strong interaction between the Pd 4d and H 1s orbitals, the 4d density of states (DOS) is modified and contains appropriate electron states, which can be utilized to stabilize the related reaction intermediates; (iii) the downshift of the *d*-band center induced by the reduced DOS near the Fermi level, resulting in the weakening binding strength between the PdH_x surface and reaction adsorbates; (iv) since the electrochemical reaction activity strongly depends on the surface atomic arrangement, different active facets possess different binding strengths for key reaction intermediates, which means the surface structure regulation of Pd-based catalysts holds an outstanding ability to improve the electrocatalytic performance.

From the viewpoint of reaction kinetics, it is necessary to deepen understanding of the relevance between surface/electronic structure and electrocatalytic activity, thereby optimizing the electrocatalytic performance of the Pd-based hydrides. According to the discussions above, a reliable conclusion is drawn that the moderate binding strength is a key parameter of electrocatalytic reaction and is related to local composition, surface structure, and strain in metal particles. In terms of optimizing the catalytic performance of Pd-based hydrides, the strategies, including previously mentioned interface engineering, electronic effect, and crystal-facets controlling, have been widely studied for promoting the intrinsic activity of each active site by electronic regulation. Notably, a surface lattice strain strategy based on lattice expansion or compression has also attracted great attention. In this regard, Liu *et al.* designed a novel core-shell $PdH_{0.43}$@Pt nanoparticles for highly efficient electrocatalytic alcohol oxidation (AOR), using cubic and octahedral Pd NPs as the cores for epitaxial growth of ultrathin Pt shells with further hydrogenation to obtain the final product [Figure 4A][35]. Benefiting from the synergism of strain effect-induced Pd lattice expansion, ligand effect, and geometric effect, the OH adsorption on the Pt surface could be strengthened. As a result, both octahedral

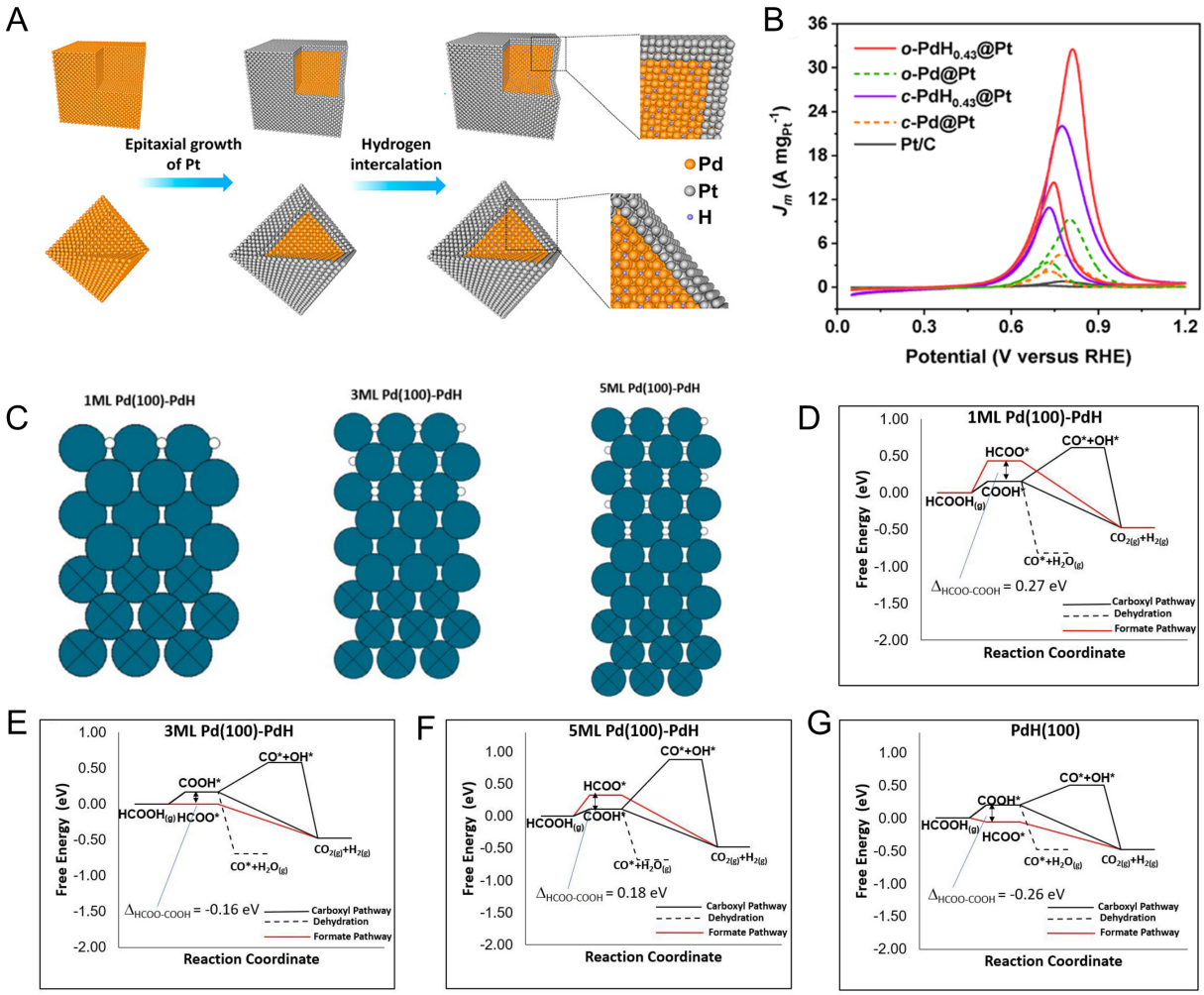

Figure 4. Lattice strain effect applied in Pd-based hydrides. (A) Schematic diagram of core-shell $PdH_{0.43}$@Pt nanostructures; (B) MOR performance of different electrocatalysts measured in 1.0 M KOH + 1.0 M methanol; (A and B) reproduced with permission from[35]. Copyright 2021, American Chemical Society; (C) the slab models with different PdH overlayer thicknesses. Diagram of FAOR process free energy on different PdH overlayer thicknesses: (D) 1 monolayer; (E) 3 monolayer; (F) 5 monolayer; and (G) 0 monolayer; (C-G) reproduced with permission from[37]: Copyright 2022, American Chemical Society.

$PdH_{0.43}$@Pt (o-$PdH_{0.43}$@Pt) and cubic $PdH_{0.43}$@Pt (c-$PdH_{0.43}$@Pt) display remarkably improved MOR activities compared to their counterparts in 0.1 M KOH [Figure 4B]. Given the combination of the two strategies of strain engineering and bimetallic hydride, this work would open an exciting avenue to expand the family of efficient PdMH electrocatalysts for electrocatalysis and beyond.

Meanwhile, we should also concern that the strain induced by the lattice mismatch is also dependent on the overlayer thickness on the substrate[70,71]. To gain a deeper insight into the relevance between strain tuning with PdH_x catalysts toward a variety of potential applications, Shi *et al.* employed first-principles DFT calculation to shed light on the effect of the hydride overlayer thickness on the FAOR reaction mechanism[37]. Through utilizing the energy difference between HCOO* and COOH* ($\Delta_{HCOO-COOH}$) as a descriptor for the preferred FAOR pathway, where positive (negative) values indicate preferential stabilization of COOH* (HCOO*). It was found that the different thicknesses of PdH overlayers on Pd (100) in the slap models, as shown in Figure 4C, enable it to affect the preferred FAOR pathway. As shown in Figure 4D-F, the corresponding DFT calculations suggest that the formation of CO* from COOH* was

preferred over COOH's dehydrogenation when 1 or 5 overlayers of PdH are supported on Pd (100). Instead, HCOO* was preferred over COOH* when the Pd (100)-PdH slap model with 3 monolayer PdH overlayers. This result indicates that the carboxyl-mediated pathway was preferred on very thin or thick PdH overlayers. More interestingly, the first dehydrogenation step for this Pd (100)-PdH was always potential-determining while it was exergonic in the case of PdH (100) as a model for pure $PdH_{0.706}$ [Figure 4G]. The authors explained that the situation is due to the release of the compressive strain which was exerted on PdH by the underlying Pd lattice in the case of Pd-PdH models. Considering the above results, it is expected that the formation of thin overlayers would play an important role in further enhancing the performance of PdH_x catalysts without changing the loading of Pd.

To better illustrate the catalytic mechanism of introducing the H atom into Pd-based materials, a relatively complete picture of enhancing catalytic performance in Pd-H systems is presented according to the above discussion. On the one hand, with the interstitial H doping, the Pd 3*d* core level spectrum of PdH_x was shifted to a higher binding energy and its valence band spectrum presented a decreased bandwidth due to the charge transfer between filled Pd 4*d* orbital and half-empty H 1*s* orbitals. Meanwhile, the Pd-Pd lattice spacing becomes to be large. The changes in the lattice parameter and charge transfer between the host and guest improve the catalytic activity and selectivity. On the other hand, the different strategies including PdMH nanostructures, strain effect, and facet design, bring many possible opportunities for Pd-based hydrides to improve catalytic performance. As one of the most classical metal hydrides, controllable synthesis of PdH_x with different structures and stoichiometric ratios by controlling the reaction conditions and the type of H source has always attracted much attention, and the current research on this aspect is still ongoing. Given the important roles of the PdH_x nanocatalysts as electrocatalysts, we believe that their synthesis and application will receive more attention and efforts in the future.

B-doped Pd-based nanocrystals

Similar to the incorporation of H atoms, B atoms could also effectively enter into the lattice sites of the host Pd[72-76]. Firstly, the B atoms have a smaller ionic radius than Pd, which would cause the enlarged Pd-Pd lattice spacing. Meanwhile, B atoms usually serve as the electron donator, which can lead to further shrinkage of the size of the B atoms and thus favor their doping in the interstices of the Pd lattice. The interstitial Pd-based borides have been widely reported to possess superior activity and excellent long-term stabilities in electrocatalysis, based on monometallic Pd being prone to deactivation with time because of surface poisoning[77]. In considering the structure-property relationship, alloying B atoms not only directly optimizes the surface electronic stages of Pd, which alter the electron density to weaken the affinity of poisoning intermediates on the Pd surface, but also facilitates the formation of BO_x and consequently accelerates the removal and further oxidation of poisoning intermediates on Pd[5,10,78-80].

The common synthetic pathways of Pd-based borides and their corresponding applications are summarized in Table 2. Particularly, most Pd-based borides were usually prepared by wet chemical synthesis, which can be divided into two basic methods: one-step and two-step approaches. Typically, the latter method possesses a better shape-controlling capability since it involves the first synthesis of Pd-based crystals with specific morphologies as precursors, followed by the introduction of B atoms to form interstitial Pd-B alloys. However, the one-step synthesis approach is simple and facile because it only involves a direct chemical reaction between Pd-containing salts and B-containing agents under hydrothermal or solvothermal conditions. Apparently, dimethylamine borane (DMAB), borane tetrahydrofuran (BH_3-THF), $NaBH_4$, and H_3BO_3 have been demonstrated to be used as effective boron sources. Besides wet chemical synthesis, the structurally ordered intermetallic Pd-B nanocatalysts can also be formed by the solid-state reaction, which can only generate at high temperatures (usually above 500 °C). Such a high temperature usually led to uncontrolled crystallization and/or mixed-phase products.

Table 2. List of common B sources and electrocatalytic applications of Pd-based borides

Catalysts	B source	Synthetic route	Electrolyte	Performance	Ref.
EOR					
Pd-B NWs	DMAB	One-step aqueous reduction	1.0 M KOH + 1.0 M C_2H_5OH	MA = 3.39 A mg^{-1}; ECSA = 41.1 m^2 g_{Pd}^{-1}	[81]
PdCuB@N-G NPs	DMAB	One-step aqueous reduction	1.0 M KOH + 1.0 M C_2H_5OH	MA = 5.83 A mg^{-1}	[82]
mesoPd-B NSs	H_3BO_3	One-step aqueous reduction	1.0 M KOH + 1.0 M C_2H_5OH	MA = 2.95 A mg^{-1}; SA = 11.3 mA cm^{-2}	[83]
ORR					
B-doped Pd NPs	DMAB	Two-step chemical syntheses	0.1 M KOH	$E_{1/2}$ = 0.86 V; MA = 2.38 mA mg^{-1} at 0.85 V; SA = 4.13 mA cm^{-2} at 0.85 V	[23]
B-Pd/C	$NaBH_4$	Two-step chemical syntheses	0.1 M KOH	$E_{1/2}$ = 0.93 V; MA = 0.97 A mg^{-1} at 0.9 V; SA = 1.27 mA cm^{-2} at 0.9 V	[84]
B-Pd/C	DMAB	Two-step chemical syntheses	0.1 M $HClO_4$	$E_{1/2}$ = 0.85 V; MA = 0.055 A mg^{-1} at 0.9 V; SA = 0.064 mA cm^{-2} at 0.9 V	[76]
FAOR					
B-doped Pd NPs	DMAB	One-step aqueous reduction	0.5 M HCOOH + 0.5 M H_2SO_4	SA = 65.4 mA cm^{-2} at 0.19 V	[78]
B-doped Pd NPs	DMAB	One-step aqueous reduction	0.5 M HCOOH + 0.5 M KOH	SA = 74.1 mA cm^{-2} at 0.35V	[85]
CO_2RR					
Pd-B films	DMAB	Electrochemical deposition	0.1 M $KHCO_3$	Product: formate, CO, and H_2; $FE_{formate}$ = 83.5% at -0.1V	[21]
B-doped Pd NPs	DMAB	One-step aqueous reduction	0.1 M $KHCO_3$	Product: formate, CO, and H_2; $FE_{formate}$ = 70% at -0.5V	[86]

As a whole, most of the binary Pd-B alloys developed previously still consist of 0D structures such as nanoparticles or nanocubes[23,72,84,86,87], which limit their potential electrocatalytic applications that are susceptible to more sophisticated nanostructures. This is partly because of the unusual reduction kinetics of the system, where the infiltration of interstitial B atoms into the Pd lattice is usually required a highly activated process under extreme conditions that may lead to the sintering of high-surface metal nanoparticles. To this end, one of the urgent desires for extending the applications of Pd-B alloy nanocatalysts is to develop a simple yet efficient route that endows the positive synergies, including binary Pd-B alloy composition and nanostructural effects.

Generally, template methods are deemed to be the most effective for controlling the growth of binary Pd-B mesoporous alloys. Lv *et al.* demonstrated the Pd-B highly ordered mesoporous structures with an atomically ordered crystal-phase sequence obtained using mesoPd/KIT-6 hybrids as the synergistic template[88]. Notably, the authors emphasized that the mesoPd/KIT-6 hybrids as the synergistic template could endow Pd-B nanoparticles with extremely mesoporous structural stability in the process of crystal phase evolution as the strong nanoconfinement effect of mesoPd/KIT-6 hybrids. It was found that the *fcc*-to-*hcp* crystal-phase transformation of mesoPd-B was achieved by interstitially inserting metallic B atoms into Pd crystals that are confined within a mesoporous silica template. Interestingly, this template-induced synthetic strategy can also be extended to other binary Pd-B alloy NWs with precisely controlled crystal structures. One notable example is given by Wang *et al.*, who reported ultrathin PdB alloy nanowires (NWs) with 1D wavy nanostructures and abundant crystalline defects as a highly active AOR electrocatalyst through a general yet straightforward surfactant-assisted aqueous synthesis[81]. The formation processes of binary PdB alloy NWs were schematically illustrated in Figure 5A. The amphiphilic surfactant, hexadecylpyridinium chloride [$C_{16}H_{33}$-pyridyl (Cl^-), C_{16}-py] were first utilized as soft functional templates

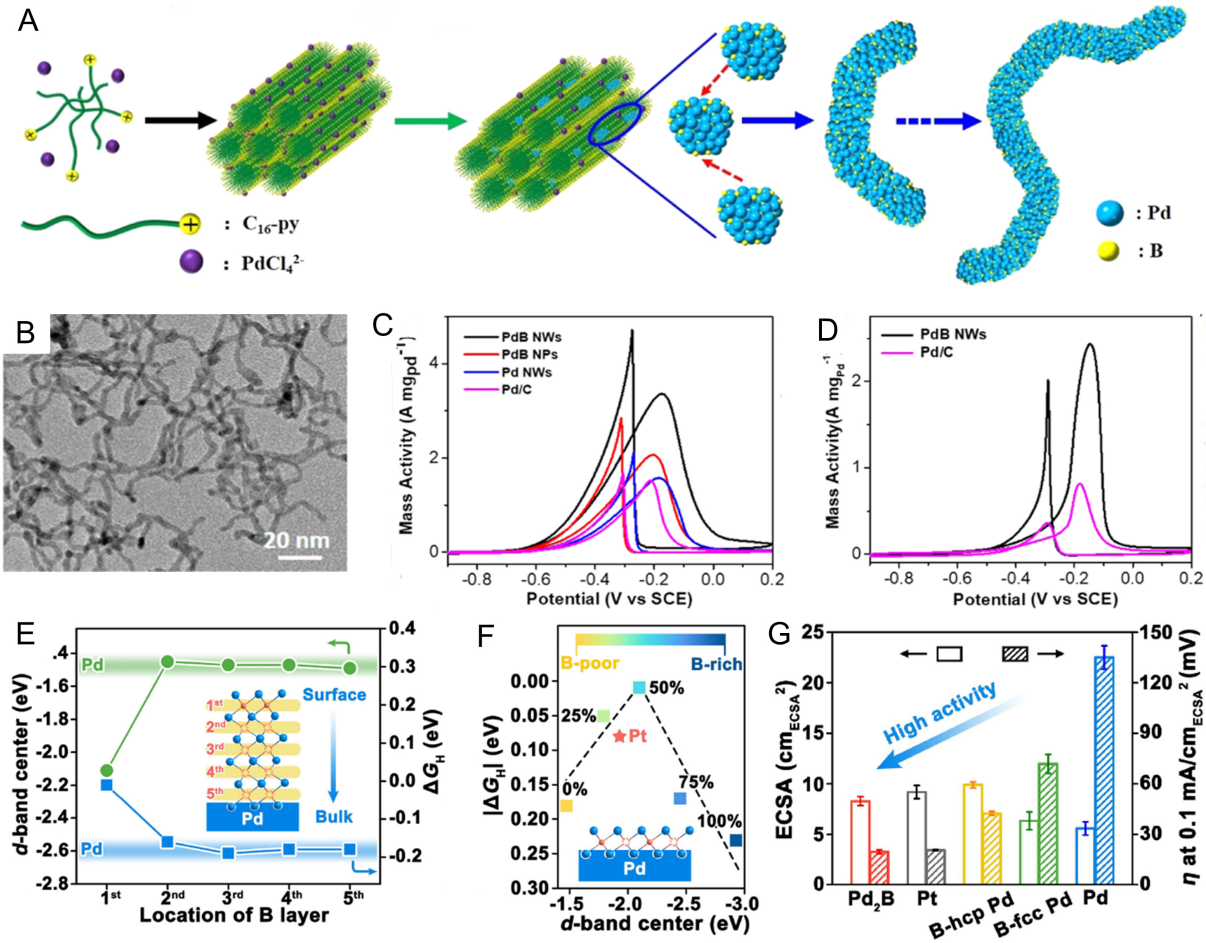

Figure 5. Growth strategy and performance influencing factors of Pd-B alloys. (A) Diagram of template-assisted aqueous growth of binary PdB nanowires; (B) low-magnification TEM image of the binary PdB NWs; (C) EOR and (D) MOR curves of binary PdB NWs and other counterparts in 1.0 M KOH + 1.0 M C_2H_5OH or CH_3OH; (A-D) reproduced with permission from[81]: Copyright 2021, American Chemical Society; (E) the relation between the B atoms location, the ΔG_{H^*} and *d* center of PdB alloy; (F) the relation between the subsurface B atoms concentration, the ΔG_{H^*} and *d* center of PdB alloy; (G) the ECSA and ECSA-normalized HER specific activities of Pd_2B catalysts and corresponding counterparts; (E-G) reproduced with permission from[89]: Copyright 2021, The Royal Society of Chemistry.

that can self-assemble with Pd precursor into a columnar mesoscopic, resulting in directing in-the-columnar growth of 1D ultrathin PdB alloy NWs along assembled columnar mesophases. Low-magnification transmission electron microscopy (TEM) shown in Figure 5B clearly demonstrates a wavy NW morphology with an ultrathin diameter and many crystalline kinks. Benefiting from the synergistic effects of binary PdB alloy composition and an ultrathin and defect-controlled NW structure, the PdB NWs exhibit outstanding EOR/MOR performance [Figure 5C-D] with the highest mass activity (3.39 A mg_{Pd}^{-1}) and excellent long-term stability in the alkaline mediums. Compared with 0D NPs, 1D ultrathin NWs can offer multiple advantages, including inhibition of the Oswald ripening process, easy accessibility of active sites, and accelerated electron/mass transfer.

Such nanostructure/morphology engineering strategy can be reliably expanded to generate ternary composition PdMB mesoporous nanosheets (MNSs), leading to enhanced electrocatalytic activity toward EOR. Introducing an additional transitional metal (such as Cu, Ag, and Pt) into the Pd-B alloy system is believed to give rise to a synergic composition effect, which enables a remarkable boost in the catalytic performance. In this respect, Sun *et al.* reported a facile *in situ* reduction strategy to prepare the ternary

PdCuB alloy nanoparticles that were stabilized on the nitrogen-functionalized graphene (N-G), and applied in the EOR[82]. The introduction of Cu weakens the adsorption affinity of ethoxy intermediates (such as CH_3COO_{ads}, CH_3CO_{ads}, etc.) and consequently accelerates the rate-determining step of EOR electrocatalysis. Moreover, the interstitial insertion of B not only directly optimizes the surface electronic structure of Pd that facilitates the desorption of Pd-O on the nanocatalyst, but also favors the functional adsorption of OH_{ads} that kinetically accelerates the further oxidation of poisoning ethoxy intermediates on Pd/Cu. It is noteworthy that the nitrogen-functionalized graphene stabilizes PdCuB nanoparticles and suppresses physical Ostwald ripening process. Compared with the PdCu alloy, the optimized PdCuB@N-G nanocatalyst exhibited excellent electrochemical EOR activity (5.83 A mg_{Pd}^{-1}) and good cycling stability. Considering the above contributions, these investigations definitely confirmed that the nanostructures engineering strategy and B alloying efficiently improved electrocatalytic performance. Importantly, it provides new insight into rationally designing and preparing high-performance Pd-B alloy nanocatalysts with various nanostructures and multicomponent features.

Apart from the various nanostructures that were synthesized to expose abundant active sites, the location, concentration, and ordering of interstitial B atoms in Pd-B alloy's near-surface (several atomic layers below the surface) are also extremely important factors for realizing excellent catalytic performance. Most investigations about binary Pd-B alloys have consistently concluded that the adsorption strength of adsorbates weakens; however, elucidation of the correlation between catalytic activity and the location, concentration and ordering of interstitial B atoms in Pd-B alloy's near-surface region has been controversial[23,79,83,84,90]. One widely accepted explanation for the correlation is that the subsurface B atoms located in octahedral interstitial sites with a half-filled state play an essential role in ensuring an appropriate degree of interatomic B(*s*,*p*)-Pd(*d*) orbital hybridization, which would downshift the *d*-band center of the Pd surface relative to the Fermi level (E_F), resulting in the modified surface adsorption and catalytic properties of binary Pd-B alloys[89,91]. For instance, Li *et al.* investigated the effects of the distribution, amount, and ordering degree of interstitial B on the HER activity of Pd-B alloy electrocatalysts[89]. Based on DFT results [Figure 5E-F], the 1st B layer (*i.e.*, subsurface B layer) in the Pd-B model brings about a much more positive Pd *d*-band center and a significant weakening of surface hydrogen adsorption energy than metallic Pd, while the deeper B layers (*i.e.*, 2nd-5st B layers) have little influence on surface Pd d-band center and hydrogen adsorption. Meanwhile, with the subsurface B concentration ranging from 0 to 100%, the surface d-band shifts down from -1.5 to -2.9 eV relative to E_F, and hydrogen adsorption becomes weaker. Note that there is a volcano-type relationship between catalytic activity and the concentration of subsurface B in the Pd lattice. The Pd-B alloy model with abundant subsurface B shows an extremely strong hydrogen binding ability that is located in the right leg of the volcano plot, while those with very little subsurface B possess too weak hydrogen binding ability that is located in the left leg of the volcano plot. Impressively, as confirmed by the intermetallic boride Pd_2B, the Pd-B alloy model with a subsurface B half-filling state at the top of the volcano plot holds an optimal HER activity. In this case, the intermetallic boride Pd_2B alloy exhibits a near-zero ΔG_{H^*} value. As shown in Figure 5G, the *hcp*-Pd_2B with interstitial B ordering displayed superior catalytic activity and stability toward HER relative to the B-doped hcp and *fcc* Pd with disordered interstitial B atoms (*i.e.*, B-*hcp* Pd and B-*fcc* Pd).

Considering the above results, the location, concentration and ordering of interstitial B atoms in Pd-B alloy catalysts play an essential role in giving rise to optimal near-surface electronic structure and adsorption properties. Despite their importance, the general realization of interstitial B atoms located in sub-surface octahedral sites with a half-filled state remains a challenge. Therefore, more work on Pd-B nanocatalysts is still required, not only to develop efficient approaches for preparing Pd-B nanocatalysts but also to comprehensively understand the modified electronic structures and surface adsorptions of Pd-B electrocatalysts.

C-doped Pd-based nanocrystals

It has been a paradigm for a long that carbon species formed *in situ* during the electrocatalytic reaction acts as adverse factors for noble metal catalysts. In earlier studies on noble metals as heterogeneous and homogeneous catalysts, carbonaceous deposits on the metal surfaces via the decomposition of reactants can strongly inhibit the catalytic activity, resulting from the sufficient blockage of metal catalytic sites caused by the carbon layers on metal surfaces. With the deepening understanding of surface science, however, it has been recently reported that carbon species can act as electrocatalyst promoters under certain conditions. The octahedral interstitial sites of Pd crystals were occupied by the C atoms and accompanied by an expansion of lattice. Also, the subsurface C atoms in the palladium carbides (PdC_x) species were likely to modify the surface electronic structure of Pd[92].

While subsurface C chemistry is proposed to promote the electrocatalytic performance of PdC_x catalysts, incorporating C atoms into Pd lattices to form PdC_x nanocatalysts remains an arduous challenge. In general, the PdC_x nanocatalysts are synthesized by following several synthetic routes: (i) calcination method, which mainly involves the gas-solid reaction between Pd black or supported Pd nanoparticles and C-containing gas (e.g., CO, C_2H_2, C_2H_4 or hydrocarbons) at temperatures above 150 ˚C [Figure 6A][93-97]. These gaseous C-containing species are supplied from the fragmentation of C-containing feed molecules, which have been observed in the conditions of acetylation, hydrogenation, and isomerization of unsaturated hydrocarbons[92,97-99]; (ii) the direct interaction of Pd nanoparticles with carbon from the C-containing support to form a PdC_x phase at 250-400 ºC under the H_2 or inert atmosphere [Figure 6A][97,100-103] One of the typically related investigations supported by the data of chemisorption and *in situ* X-ray diffraction has indicated the formation of a carburized Pd phase as a result of the interaction of Pd nanoparticles with carbon support[103]; (iii) one-step chemical reduction of Pd salt in the presence of an organic additive. Such a preparation method has been employed by Okitsu and Takuo in the synthesis of PdC_x using tetrachloropalladate (II) or tetracyanoethylene[104,105]; (iv) treating the prepared Pd crystals as the precursors to carbonize with organics like Na_2EDTA or glucose under hydrothermal/solvothermal conditions[106,107]. This method has been shown the capability to constructing PdC_x nanocrystals with tunable C/Pd atomic ratios by simply adjusting the reaction time, and it is considered to be more suitable for preparing PdC_x nanocrystals than the aforementioned methods that might require extreme conditions like high temperature and/or pressure. Regardless of the carbon source, the surface electronic structure and adsorption properties of Pd generate a substantial change through the presence of surface PdC_x species formed by carbon dissolving into the subsurface of Pd nanoparticles, illustrating the potentially positive roles of carbon in catalysts, as demonstrated by some theoretical and experimental studies[92,97]. As a quintessential example, Simonov *et al.* prepared the PdC_x/XC72 catalyst as a highly efficient electrocatalyst for the HOR by the migration of C atoms from the support to Pd lattices [Figure 6A-B][97]. Under the influence of incorporated C atoms, the weakened CO adsorption on Pd carbide and the absence of H absorption have been achieved, increasing the number of active sites for the HOR. The promoting effect of the incorporated C atoms is supported by a control experiment to remove the doped carbon from the Pd lattice by oxygen treatment at 300 °C. As shown in Figure 6C, the PdC_x/XC72 catalyst subjected to the oxidative treatment (dashed line) has a notable decrease in the exchange current density of HOR compared with the PdC_x/XC72 (solid line) under the same specific Pd surface area of 2.5 cm^{-2} (geom.), implying a drop in catalytic activity. In this study, the process of CO adsorption on Pd modified with incorporated C atoms was found to be partially suppressed, indicating an enhancement in CO tolerance. In other words, an increase in the number of active sites for the HOR was obtained in PdC_x/XC72 catalyst, leading to a significantly enhanced current density of the HOR. This work further confirmed the promoting effect of incorporated C atoms. It is worth mentioning that the promoting effect of subsurface C atoms is not a particular feature of Pd, but a common feature for noble metals such as Ag and Au[108].

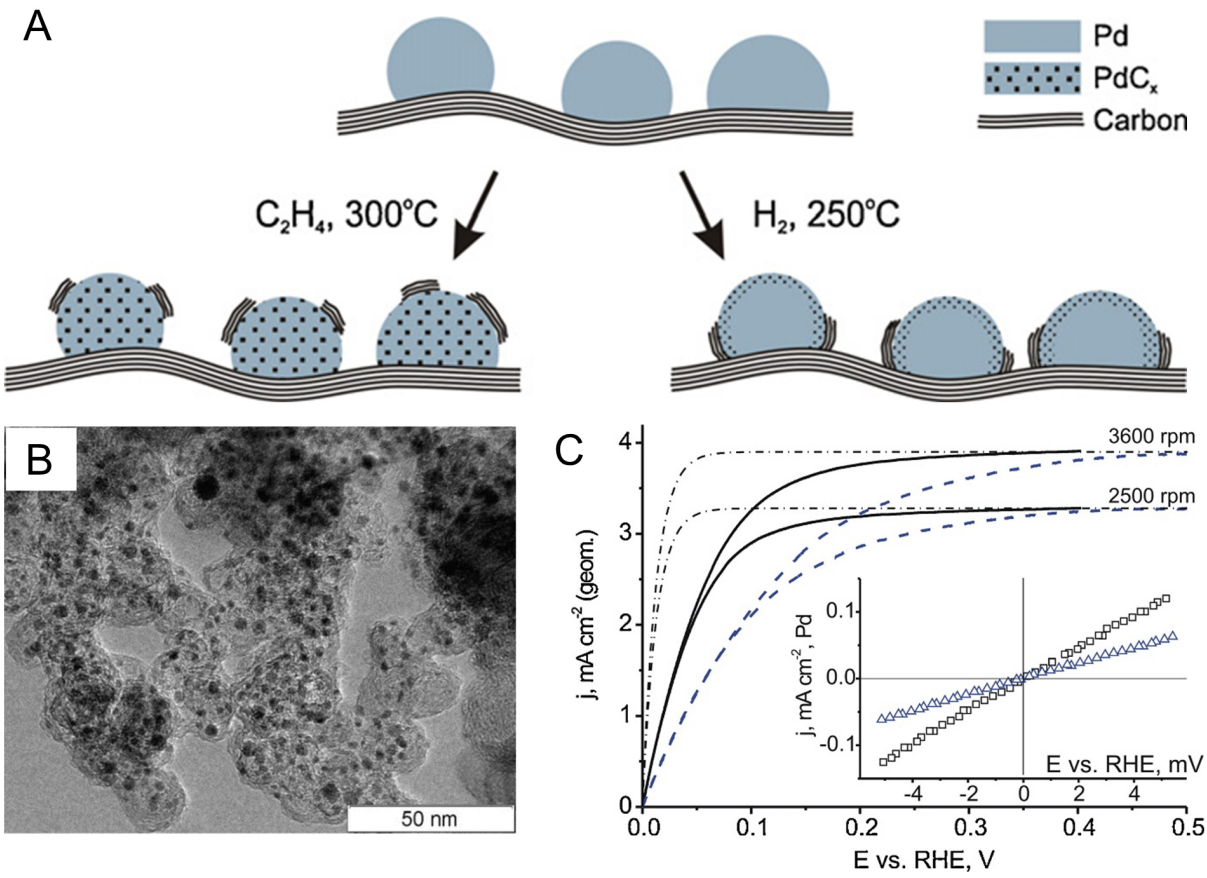

Figure 6. Synthesis strategy and positive influence of surface PdC_x species. (A) Two typical routes for incorporating C atoms into Pd lattices; (B) TEM image of the PdC_x/XC72 catalyst; (C) the comparison of exchange current density of HOR over the PdC_x/XC72 (solid line) and oxygen-treated PdC_x/XC72 (dashed line); (A-C) reproduced with permission from[97]: Copyright 2012, Elsevier.

Adjustable C/Pd atomic ratios is a feasible strategy to create new PdC_x to realize optimal catalytic activity and selectivity for certain reaction. However, the precision synthesis of the controlling composition of Pd and C within PdC_x nanocatalysts has been scarcely reported, greatly because the preparations aforementioned usually require harsh conditions or rely on a particular substrate. These limitations have hindered the investigation of the effect of C content on electrocatalytic performance. Given this fact and the harsh synthetic conditions (such as high temperature/pressure) required in other approaches, more research is needed to develop an effective and environment-friendly method with mild synthetic conditions for the preparation of PdC_x catalysts.

N-doped Pd-based nanocrystals

Palladium-based nitrides (PdN_x) as non-stoichiometric and interstitial compounds could also form via the N atoms filling into the octahedral interstitial sites within Pd lattices. The addition of N could be expected to impart Pd-based catalysts with better electrocatalytic performance as a result of the unique properties of metal nitrides, such as high resistance against corrosion, high hardness, high melting points, density and low electrical resistance[109-111]. The synthesis of Pd-based nitrides, however, has long posed one of the biggest challenges in efficient electrocatalysts applications because of the predicted low metal-N bond strength and the generally unreactive nature of the most readily available nitrogen sources (e.g., N_2, NH_3, ammonia, and

amides) at low and moderate temperatures[112,113]. Generally, metal nitrides are often prepared by following several synthetic pathways: (i) subjecting corresponding metal oxides to heating in flowing NH_3 by slowly raising the temperature[114-116]; (ii) heating treatment metals or samples combined with carbon-based materials to high temperatures in N_2 or NH_3 environment[117,118]; (iii) calcining along with nitrogen-based compounds, which involves the ammonolysis of binary compounds that often produces nitrides[119,120]; (iv) high temperature/pressure approaches are often used to synthesize metal nitrides[121,122]; (v) some other approaches include vapor deposition techniques[110,123], solid-state metathesis[124], solvothermal synthesis[125], and sol-gel processing[126]. Unfortunately, most of these methods are focused on the synthesis of transition metal nitrides, and there are relatively few reports on the synthesis of noble metal nitrides because the precious metal-N bonds are difficult to create. Additionally, some methods sometimes are considered unfriendly to the environment due to the use of toxic nitrogen sources and high temperatures. Hence, much improvement is still needed to access the PdN_x via using the above methods, resulting in urgent demand for facile, effective, and environmental-friendly methods to synthesize the PdN_x catalysts. Moreover, controlling the morphology and nitrogen content of some PdN_x nanocrystals during their preparation has also attracted much attention. One of the related studies was reported by Veith *et al.*[127] They developed an effective formation strategy of N-rich Pd nanoparticles via reactive sputtering of the pure metal in the N_2 plasma. Through controlling the particle size and deposition condition (pressure, power, and distance), the stoichiometry of the as-prepared PdN_x nanoparticles is $PdN_{6.7}$ (87 at % N), in which the high concentration of N ligands increases the electrochemical stability *via* blocking all active sites. This result proves the potential of N to influence the properties of precious metal materials in a favorable way, and the premise is to develop appropriate synthesis methods.

Although the importance of interstitial N atoms for regulating the activity and stability of catalysis has been verified, PdN_x nanostructures with controllable stoichiometries are difficult to control experimentally. This seriously hinders the understanding of the structure-activity relationship between interstitial nitrogen content and catalyst performance. A widely accepted explanation is that the interactions between the N *p* and Pd *d* orbitals might be strongly associated with the structure-activity relationship. As a further example, Guo *et al.* recently demonstrated the synthesis of PdN_x nanocrystals ($x \leq 0.5$) with controllable stoichiometric via the hydrothermal decomposition of urea to incorporate N atoms into the lattices of Pd nanocubes [Figure 7A][128]. Corresponding EDS images clearly reveal the effective doping of N atoms. The concentration of the urea could be changed to adjust the chemical stoichiometries of PdN_x nanocrystals. The obtained PdN_x nanocrystals not only exhibit superior catalytic performance for FAOR and MOR, but also offer an impressive ORR catalytic activity in 0.1 M KOH [Figure 7B], in which the Pd_2N nanocrystals show the most positive potential compared with all catalysts. More importantly, after accelerated durability tests (ADTs) of 10,000 cycles [Figure 7C], it was further demonstrated that the excellent cycling stability of Pd_2N nanocrystals toward ORR with activity decay only ~9%. Regarding the enhancement mechanism, the authors found that the strong interactions between Pd and interstitial N atoms cause a downshift and optimization of the Pd *d*-band center, thus improving the electrocatalytic activity and stability. It should be worth noting that there is an obvious dependence of catalytic activity on the N/Pd ratio, suggesting the pronounced effect of proper N content on enhancing the catalytic performance of noble metal nanocatalysts. In particular, the *d*-band center of the PdN_x nanocrystals will decrease with the increase of N filling concentration, which is believed to benefit the removal of absorbed O and OH species and thereby improve the catalytic performance toward ORR[131]. It is widely accepted that this dependence on N filling concentration may be attributed to factors such as structure and electronic effects[132,133]. As noted in the example above, the modified electronic structure, polycrystalline structure containing plenty of dislocation and grain boundaries can lower the *d*-band center position of Pd and provide extra active sites, resulting in a deep understanding of the correlation between the nitrogen content and the catalytic performance. Such correlation may be a combination of electronic and/or structural effects.

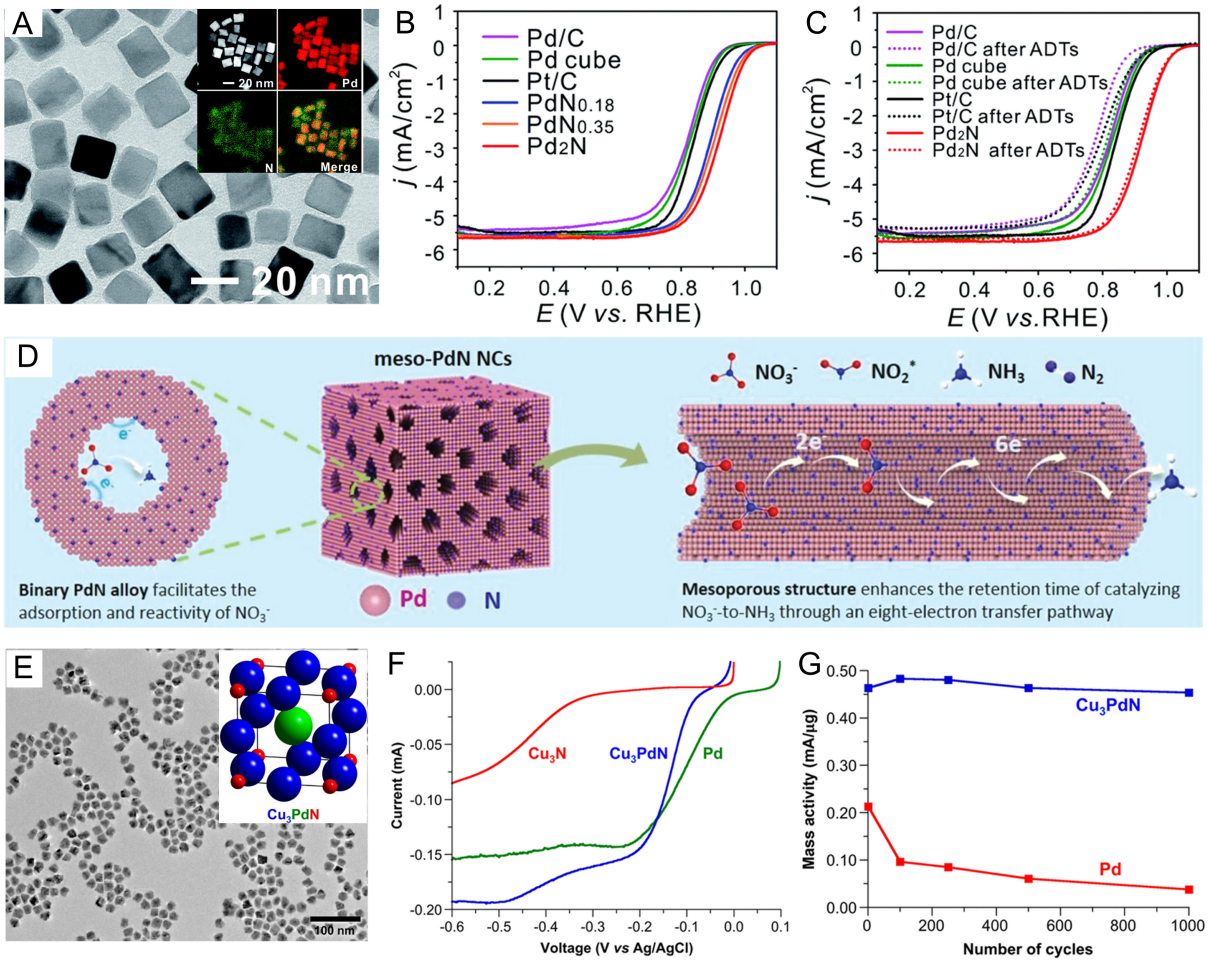

Figure 7. Effect of composition proportion and structure design on the electrocatalytic performance of Pd-based nitrides. (A) TEM image of Pd_2N nanocrystal with inset EDS mappings diagram; (B) ORR polarization curves in 0.1 M KOH of Pd-based nitrides with different nitrogen content and other counterparts; (C) the stability tests of the catalysts in Figure 7B; (A-C) reproduced with permission from[128]: Copyright 2021, The Royal Society of Chemistry; (D) diagram of the electrocatalytic mechanism of meso-PdN NCs for selective NO_3- to -NH_3 electrocatalysis. Reproduced with permission from[129]: Copyright 2022, Wiley-VCH; (E) TEM image of Cu_3PdN nanocrystals with insert antiperovskite-type Cu_3PdN structure model; (F) ORR polarization curves of Cu_3PdN, Cu_3N, and Pd nanoparticle in 0.1 M KOH; (G) the relation between mass activity and cycle numbers of Cu_3PdN and Pd; (E-G) reproduced with permission from[130]: Copyright 2014, American Chemical Society.

Noted from the structural effects for boosting electrocatalytic performance, recent works also reveal that nanostructures of metal nitrides are often desired for improving their surface reactive properties and further expanding their applications. Sun *et al.* constructed mesoporous PdN NCs with highly penetrated mesoporous channels by treating the prefabricated meso-Pd NCs with urea under hydrothermal conditions. The mesoporous framework with abundant exposed abundant undercoordinated active sites contributes to the adsorption of NO_3^- and facilitates the subsequent reactivity of NO_3^-- to -NH_3 electrocatalysis [Figure 7D][129]. Notably, benefiting from the longer mesoporous channels and alloying N, the outward diffusion of Pd atoms is inhibited, the total reaction energy is reduced, and the retention times of the deeper electrocatalytic reduction of pre-reduced NO_2^- is increased, thereby synergistically promoting the conversion of the deeper electrocatalytic reduction of pre-reduced NO_2^-, for which synergistically facilitating subsequent six-electron reaction into NH_3 and boosting the electrocatalytic cycling stability. As a further example, Lee *et al.* prepared a novel antiperovskite-type intermetallic nitrides $(Ni_{0.3}Pd_{0.7})NNi_3$ as a highly efficient ORR electrocatalyst in acidic conditions by transforming the disordered $PdNi_3$ to long-rang-

ordered antiperovskite crystal structures under NH_3 environment with high temperature[134]. The antiperovskite structured intermetallic nitrides exhibited superior ORR activity and stability, originating from the downshift *d*-band center of the monolayer Pd/antiperovskite surface and the lower formation energy of the antiperovskite core nanocrystal. This result suggests that the unique crystal structure of antiperovskite-type nitrides is beneficial to improving the electrochemical properties, which opens an exciting avenue to expand the family of cost-effective ORR electrocatalysts. Inspired by this structure, similar improvements in ORR performance were observed in the work by Vaughn *et al.*[130] They also developed an efficient solution-phase synthesis of antiperovskite-type Cu_3PdN nanocrystals that are multifaceted with a quasi-cubic morphology [Figure 7E], through the reaction of copper(II) nitrate and palladium(II) acetylacetonate in 1-octadecene with oleylamine at 240 °C. As expected, the Cu_3PdN nanocrystals have a half-wave potential ($E_{1/2}$) value of -0.13 V, while those of the Cu_3N and Pd are -0.45 and -0.07 V [Figure 7F], suggesting the ORR activity of the Cu_3PdN nanocrystals is improved substantially relative to that of comparable Cu_3N nanocrystals but similar to that of Pd. More importantly, the repeated cycling experiment indicated that the Cu_3PdN nanocrystals show great enhancement in ORR activity and cycling stability than comparable Pd nanocrystals by constructing antiperovskite-type nitrides [Figure 7G]. According to the above discussion, the fine structure and shape control of Pd-based nitrides catalysts is a viable strategy for achieving excellent catalytic activities and durability. However, there are few examples of multi-metal Pd-based nitrides with different nanostructures. Hence, an urgent requirement for the design of advanced N-doped Pd-based catalysts to establish the fundament correlations between the composition, structure, and reactivity of Pd-base nanomaterials.

O-doped Pd-based nanocrystals

The antitoxic property has always been an essential evaluation indicator for designing high-performance Pd-based electrocatalysts. The formation of abundant palladium oxide (PdO_x) species, including palladium oxides and hydrous palladium oxides, through the oxidation treatment of Pd catalyst has been verified to be an effective strategy for improving anti-poisoning capability as a result of the excellent elimination of CO-like poisoning intermediate species[135-137]. Therefore, PdO_x-containing catalysts have drawn a rising awareness due to the crucial role of PdO_x in improving electrocatalytic properties. In general, the synthesis of Pd-based oxides can be summarized as two representative pathways: (i) The one is the oxidation treatment of the pre-reduced or existing Pd-based crystals under oxygen or air atmosphere to form PdO_x species[136-140]. For example, Hu *et al.* prepared a supported PdO nanocatalyst *via* a two-step procedure where $Pd(NO_3)_2$ was first reduced by formaldehyde and then oxidation for the removal of NO_x and CH_4[140]; (ii) Another way is a direct one-step synthesis via the thermal decomposition of the impregnated Pd^{2+} species within Pd salts in the air or a simple solvothermal method[141-143]. Wang *et al.* developed a facile high-temperature pyrolysis method to synthesize porous Pd-PdO nanotubes for methanol electrooxidation, in which Pd(II)-dimethylglyoxime complex nanorods as the pyrolysis precursor[142]. Interestingly, Guerrero-Ortega *et al.* developed a novel two-step procedure that uses organometallic $Pd(dba)_2$ rather than Pd salts as the reduced precursor to fabricate carbon-supported core-shell Pd@PdO catalyst, which exhibits the highest oxidation current magnitude during methanol electrooxidation as a result of the presence of interactions between PdO and Pd[136]. With the rapid development of synthetic technologies, there are also some other methods reported. Plasma sputtering of a Pd electrode under the oxygen atmosphere has been utilized to prepare the highly oxidized palladium (Pd^{4+}) species, which were found to be high thermal stability and high reaction probability toward CO at room temperature compared to the oxidized palladium (Pd^{2+}) species[144]. Moreover, Kuriganova *et al.* have also proposed a new electrochemical dispersion approach of a Pd foil electrode under pulsed alternating current conditions for the preparation of the Pd-PdO/C electrocatalyst toward formic acid oxidation[145].

Regardless of the synthesis routes, the as-prepared O-doped Pd-based catalysts display better electrocatalytic activity and durability as a result of the valid O doping. On the one hand, the abundant PdO_x species on the surface of the Pd-based oxide electrocatalysts can provide the required oxygen species for the oxidation of CO-like poisoning intermediate, leading to significantly improved poisoning tolerance and consequently retard the attenuation of electrocatalysts[135-137,146]. On the other hand, the strong interface interaction between Pd and PdO_x species has been confirmed to induce charge redistribution and influence the adsorption behavior of the reaction intermediates. The strong interface interaction can also be contributed to the significantly enhanced electrocatalytic activity and stability of catalysts[147-150]. Meanwhile, Xing *et al.* have conducted related explorations about the roles of the Pd-PdO interface[148,149]. The combination of designed experiments, DFT calculations, and *in situ* sensitive probes demonstrated that the Pd^0 sites achieve the activation of formic acid and the adsorption of active intermediate, while the Pd^{2+} sites pull hydrogen from the reaction intermediates, and the Pd/PdO heterojunction overcomes the CO poisoning by eliminating the dehydration pathway. These results strongly confirmed that the presence of the Pd-PdO interface plays a decisive role in formic acid dehydrogenation. Interestingly, the authors shed light on the regulation of the Pd-PdO interface by introducing polyaniline as nanoparticles support, which was found to be an electronic structure modulator for metal particles. As a result, the amount of Pd-PdO interface is increased owing to the polyaniline modification, thus contributing to increased catalytic activity[148].

Noted from the promising interface interaction between Pd and PdO for electrochemical reactions, recent works also reveal that the formation of Pd-PdO interfacial structure is a feasible way to solve dynamic issues during the NRR process. As investigated by Lv *et al.*, PdO/Pd heterojunctions supported on carbon nanotubes (PdO/Pd/CNTs) were constructed by reducing PdO/CNTs with ultraviolet laser irradiation, while the abundant PdO–Pd interfaces can act as active sites for N_2 dynamic activation and proton transitions [Figure 8A][150]. Benefitting from the synergistic effect of Pd and PdO, the transmission route of H protons and activated N_2 was greatly decreased, thereby ensuring that the electrocatalytic NRR efficiency was significantly improved. Under the influence of the PdO–Pd interfaces, the N_2 adsorbed on the Pd surface can sufficiently form chemisorbed Pd-N bonds, while PdO can adsorb H protons located in the subsurface region to imitate α-PdH. It should be noted that the reduction degree of PdO and optimum ratio of Pd/PdO are critical for the best catalytic activity. As the irradiation process proceeded, the 10 min irradiated PdO/Pd/CNTs presented an optimal mass ratio of Pd (18%) to PdO (82%) and the highest NH_3 yield rate of 18.2 μg $mg_{cat.}^{-1}$ h^{-1} [Figure 8B], indicating that the PdO/Pd/CNTs (10 min irradiation) reduce the overpotential of the chemical reaction, as verified by the HER curves [Figure 8C]. These results not only demonstrate that the presence of Pd-PdO interfaces plays a critical role in enhancing the catalytic NRR performance but also open an exciting avenue to design high-performance PdO/Pd-based nanocatalysts as the NRR electrocatalysts.

Considering the importance of the Pd-PdO interface, some design strategies have been demonstrated to boost the catalytic efficiency of PdO/Pd-based nanocatalysts by a combination of constructing Pd-PdO interfaces and incorporating appropriate supports [Table 3]. The complex interactions between Pd/PdO catalysts and their support matrixes may be strongly associated with excellent catalytic performance in several different ways: Firstly, the MO_x (M = Ce[156], Zr[153,157], Ni[158], Al[159], *etc.*) as the support can dilute the concentration of Pd atoms, thus maximizing the Pd active sites and minimizing the deactivation caused by the metal-sintering processes. Secondly, the *in-situ* reduction of activated PdO nanoparticles at high-temperature might bring about the encapsulation of Pd nanoparticles within thin and partially reduced metal oxide layers, which could stabilize the active component and avoid the aggregation of Pd-based NPs to increase the structural and electrocatalytic stability. Meanwhile, the interface between Pd and the metal oxides would also cause a change in the electronic structure, inducing the charge redistribution and

Table 3. Non-exhaustive list of common PdO/Pd support materials and their applications from recent literature

Catalysts	Synthetic routes	Support material	Electrolyte	Performance	Ref.
EOR					
Pd-PdOx@GS-NH_2	Two-step Procedure	Graphene Sheets	1 M KOH + 1 M C_2H_5OH	E_{onset} = -0.55 V (*vs.* Hg/HgO); ECSA = 24.9 $m^2 g^{-1}$	[135]
PdO/MWCNTs	Dry grinding	Multiwalled carbon nanotubes	1 M KOH + 1 M C_2H_5OH	E_{onset} = -0.70 V (*vs.* SCE); MA = 5.03 A mg^{-1}	[152]
Pd@ZrO_2/Si-Al_2O_3	Two-step procedure	Si-modified alumina	1 M KOH + 1 M C_2H_5OH	MA = 1.71 A mg^{-1}	[153]
PdO-Pd-Fe/HCSs	Pyrolysis method	Huge carbon spheres	1 M KOH + 1 M C_2H_5OH	SA = 13.3 mA cm^{-2}; ECSA = 8.03 $m^2 g^{-1}$	[154]
MOR					
Pd/PdO/PG	Plasma sputtering	Multiwalled carbon nanotubes	1 M CH_3OH + 1 M KOH	MA = 1.65 mA mg^{-1}	[147]
Pd@PdO-Co_3O_4	One-pot synthesis	Vulcan carbon (XC-72R)	1 M CH_3OH + 1 M KOH	E_{onset} = -0.37V; MA = 1.72 A mg^{-1}	[136]
NRR					
PdO/Pd/CNTs	Laser irradiation	Carbon nanotubes	0.1 M NaOH	NH_3 yield = 17.53 μg h^{-1} $mg^{-1}_{cat.}$; FE = 11.6% at -0.10 V	[150]
ORR/OER					
Pd@PdO-Co_3O_4	Two-step Procedure	ZnO Nanorod	1 M KOH	ORR:E_{onset} = 0.92 V with $E_{1/2}$ = 0.78 V; OER: η_{10} = 1.54 V	[155]

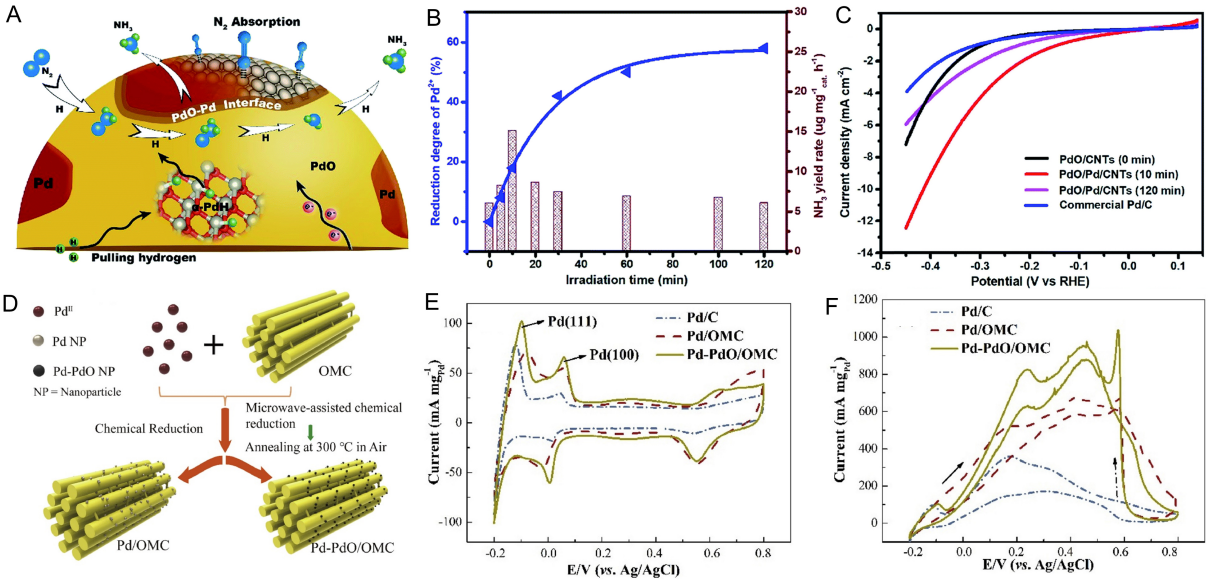

Figure 8. Effect of the Pd-PdO interfacial interaction and appropriate supports on the electrocatalytic performance of Pd-based oxides. (A) Diagram of NRR process on the Pd-PdO interface; (B) the relation between the varied irradiation times and the reduction degree (blue line) and NH_3 yield rate (brown line) of PdO/CNTs; (C) LSV curves of PdO/CNTs with different irradiation times; (A-C) reproduced with permission from[150]: Copyright 2019, The Royal Society of Chemistry; (D) diagram of the introduction of ordered mesoporous carbon over Pd/OMC and Pd-PdO/OMC catalysts. The CV curves of Pd-PdO/OMC and its counterparts measured in different solutions: (E) 0.5 M H_2SO_4 solution; (F) 0.5 M H_2SO_4 + 0.5 M HCOOH solution; (D-F) reproduced with permission from[151]: Copyright 2020, Elsevier.

ultimately improving the catalytic performance[160]. Particularly, the performance of PdO/Pd-based catalysts can also be remarkedly improved while using carbon materials as the support, including graphene[135,147,161], carbon nanotubes[152], carbon nanofibers[162], carbon nanosphere[154], and ordered mesoporous carbons[151], which have a sequential structure and high electronic conductivity. Therefore, it is highly desirable to

optimize catalytic performance by designing the PdO/Pd-support interfaces based on the above points. As a further example, Zhou *et al.*[151] developed an ordered mesoporous carbon-supported Pd-PdO catalyst (Pd-PdO/OMC) through microwave-assisted chemical reduction followed by the annealing treatment [Figure 8D], where the OMC and microwave treatment were introduced to enhance the spatial dispersion of Pd nanoparticles and reduce the negative effect of annealing process. The cyclic voltammetry results reveal that the larger hydrogen adsorption/desorption regions and the highest forward anodic current peak value are attributed to the highly dispersed and likely "confined" Pd nanoparticles on OMC as well as favorable species transport [Figure 8E-F]. Due to the abundant exposed active sites and strengthened anchoring effect of Pd-PdO catalyst on the OMC substrate, the Pd-PdO/OMC catalyst exhibits excellent activity and stability toward FAOR.

Even though considerable progress has been acquired in the supported Pd/PdO-based catalysts and their electrocatalytic applications, many questions, including the dynamic evolution of the interface between Pd/PdO and the support under experimental conditions, should be clearly defined to offer guidance for rational designing high-performance Pd/PdO-based electrocatalysts.

P-doped Pd-based nanocrystals

Since the doped P with abundant valance electrons would significantly affect the electronic states of noble metal elements, the formation of the Pd-P alloy is one of the most effective ways to modulate the intrinsic activity of Pd-based electrocatalysts[163]. The 3*d* electron density of the Pd atoms will be decreased due to the electron transfer from Pd to P caused by the higher electronegativity value of P than that of Pd, thus boosting the resultant electrocatalytic performance accordingly[164,165]. Therefore, the P-doped Pd-based nanocrystals have attracted considerable research interest to obtain superior catalytic performance toward various electrocatalytic reactions and reduce the mass loading of Pd[166,167].

Nevertheless, the synthesis of P-doped Pd-based nanocatalysts is still a tremendous challenge owing to the lack of a feasible scheme and optimal design for doping P into Pd lattices. In addition, since these methods usually contain toxic phosphorous sources, the selection of phosphorus sources is critical. By far, the representative preparation of P-doped Pd-based nanocatalysts follows three synthetic pathways: (i) liquid-phase synthesis, including the hydro-/solvothermal or water/oil-bath methods, which is a bottom-up synthesis method of Pd-based phosphides, usually generating via dissolving the Pd metal precursors and P source in the solvents[168-172]. Noted that acetylacetone salts of Pd are widely used as the Pd metal precursors while organic phosphines, such as tri-n-octylphosphine (TOP), triphenylphosphine sulfide (TPS), tri-n-octylphosphine oxide (TOPO), triphenylphosphine (TPP), and hexamethylphosphoroustriamide (HMPT) as P sources in the organic solvents. Using this approach, controlled morphologies and sizes of Pd-based phosphides can be obtained and carried out at a much lower temperature (generally at 180-300 °C), in which the C-P covalent bond of organic phosphines breaks easily to release phosphorus among the temperature range[157]. Correspondingly, Pd inorganic salts as the metal precursors with NaH_2PO_2 as the P sources are usually applied in the aqueous synthesis of Pd-based phosphides[163,173]; (ii) gas-solid reaction with a heating treatment in an inert/reducing atmosphere, in which Pd chloride salts or bulk usually serve as metal precursors while hypophosphite (e.g., NaH_2PO_2 and $NH_4H_2PO_4$) and phytic acid are widely used as P source[20,174-176]. It is noted that hypophosphite serves as a P source and may lead to poisoning and the autoignition of PH_3 under a high-temperature condition (> 500 °C), making it difficult to guarantee experimental safety[177]; (iii) other synthetic methods, including solid state reaction[167,178], stepwise electroless deposition[179] and others.

In general, the introduction of surfactants or templates can boost the potential of constructing electrocatalysts with specific morphology and composition under liquid-phase synthesis. This surfactants/templates-assisted synthetic strategy may also provide new insight into constructing other nonmetals doped Pd-based catalysts, which might be promising candidates for advanced catalytic applications. However, it should be noted that the expensive cost and a "clean" surface are required for the high-performance electrocatalysts synthesized by surfactants or templates[180]. Compared to liquid-phase synthesis, the higher temperatures in the gas-solid phase reaction facilitate the complete conversion of metals to phosphides with the convenient introduction of carbon-based materials. Unfortunately, particle agglomeration may be generated and accompanied by the performance degradation under high-temperature conditions. To better understand the effects of synthesis methods and phosphorus source selection on performance, a summary of different synthesis methods and phosphorus sources of P-doped Pd-based nanocrystals was presented in Table 4.

From the viewpoint of geometric structure, morphology has a significant influence on catalytic performance[188]. To date, researchers have reported a large number of Pd-based phosphides with various nanostructures and compositions, such as nanoparticle networks (NNs)[164], nanosheets[165,170], and amorphous nanoparticles[179] to promote the electrocatalytic performance towards a set of electrocatalytic reactions. For example, Lv *et al.* have successfully constructed the highly branched and defect-rich PdP nanosheets *via* an effective surfactant-directed aqueous synthesis, in which the surfactant docosylpyridinium bromide and its corresponding self-assembled micelles were employed as nanoreactors for the nanoconfined growth of PdP NSs [Figure 9A][165]. Under the strong nanoconfinement effect of the surfactant docosylpyridinium bromide, a well-alloyed branch framework with homogeneously distributed Pd and P was obtained, in which abundant crystallographic defects were observed. The higher integrated charge in the cathodic peak and the larger ESCA observed on the PdP NSs, are favorable for the enhancement of the electrocatalytic EOR performance [Figure 9B]. The authors explained that the ultrathin and highly branched structure contributes to the abundant exposed active sites and the P-alloyed composition induces the strong electronic interaction, which together endow the binary PdP NSs with remarkable mass activity, stability, anti-poisoning ability, and enhanced reaction kinetics towards EOR. This enhancement mechanism and effective surfactant-directed aqueous synthetic strategy are applied equally to the 3D network nanostructure. As investigated by Zhang *et al.*, a facile one-step template (*i.e.,* Brij 58) assisted aqueous growth was proposed to obtain the 3D Pd-P NNs for superior FAOR with significantly improved CO tolerance performance [Figure 9C][164]. On the one hand, 3D networks may be contributed to the exposure of intrinsic active sites. On the other hand, the presence of strong electronic interactions between Pd and P can significantly weaken the CO binding to the modified Pd surface, thus effectively reducing the overpotential for FAOR. These results strongly suggest that the synergistic structural and compositional advantages can be associated with boosted electrocatalytic performance.

Note that the role of P alloying in enhancing the catalytic performance of Pd catalysts has been proven to be a practical option. More importantly, the combined introduction of oxyphilic secondary metals M (Ni, Cu, *etc.*) and P to fabricate multicomponent nanoalloys has also become a hot research topic purposed for further optimizing and boosting the catalytic performance of Pd-based catalysts and, meanwhile, reducing the mass loadings of Pd metals[168,181-183,189]. Impressively, these Pd-M-P ternary and even quaternary catalysts can act as a class of electrocatalysts for EOR, since the oxyphilic metals can effectively accelerate the chemical absorption of OH^- and the formation of OH radicals, thus enhancing the EOR activity and CO tolerance property[181]. Recently, Lv *et al.*[182] prepared an ultrathin anisotropic multicomponent PdCuP NWs through one-pot surfactant-directing aqueous synthesis to serve the improved EOR activity and stability [Figure 9D]. On the one hand, the ultrathin NW structure could alleviate the Oswald ripening and

Table 4. List of synthesis methods and phosphorus sources for Pd-based phosphides

Catalysts	P routes	Synthetic route	Electrolyte	Performance	Ref.
EOR					
PdP_2/rGO	HMPT	Liquid-phase synthesis	0.5 M KOH + 0.5 M C_2H_5OH	SA = 1.56 mA cm^{-2}; MA = 0.05 A mg^{-1}	[157]
Pd-Ni-P NPs	TOP	Liquid-phase synthesis	1 M NaOH + 1 M C_2H_5OH	SA = 4.95 mA cm^{-2}; MA = 0.23 A mg_{Pd}^{-1}	[169]
PdNiP/C	NaH_2PO_2	Liquid-phase synthesis	0.5 M NaOH + 1 M C_2H_5OH	MA = 2.53 A mg_{Pd}^{-1}	[181]
PdP NSs	NaH_2PO_2	Liquid-phase synthesis	1 M KOH + 1 M C_2H_5OH	MA = 3.22 A mg_{Pd}^{-1}	[165]
PdCuP NWs	NaH_2PO_2	Liquid-phase synthesis	1 M KOH + 1 M C_2H_5OH	MA = 6.7 A mg_{Pd}^{-1}	[182]
Pd-Ni-P	NaH_2PO_2	Liquid-phase synthesis	0.1 M KOH + 1 M C_2H_5OH	SA = 19 mA cm^{-2}; Tafel slope = 60 mV dec^{-1}	[183]
Pd-P/3DNGS	NaH_2PO_2	Liquid-phase synthesis	1 M KOH + 1 M C_2H_5OH	ECSA = 67.9 m^2 g^{-1}; E_{onset} = -0.58 V (*vs.* Hg/HgO)	[173]
MOR					
Pd-Ni-P/C	TPP	Liquid-phase synthesis	0.5 M KOH + 1 M CH_3OH	MA = 3.3 A mg^{-1}; ECSA = 62.9 m^2 g^{-1}	[168]
Pd/P NPs	NaH_2PO_2	Liquid-phase synthesis	1 M KOH + 1 M CH_3OH	MA = 0.84 A mg^{-1}; ECSA = 50.7 m^2 g^{-1}	[170]
FAOR					
PdP/C	Red P	Solid state reaction	0.5 M HCOOH + 0.5 M H_2SO_4	SA = 1.17 mA cm^{-2}	[178]
NRR					
AuPdP NWs	$Pd(PPh_3)_4$	Liquid-phase synthesis	0.1 M Na_2SO_4	NH_3 yield = 18.78 μg h^{-1} mg_{cat}^{-1}; FE_{NH3} = 15.44%	[184]
PdP_2/rGO	Red P	Solid state reaction	0.5 M $LiClO_4$	NH_3 yield = 30.3 μg h^{-1} mg_{cat}^{-1}; FE_{NH3} = 12.56%	[167]
ORR					
PtPdNiP MNs	NaH_2PO_2	Liquid-phase synthesis	0.1 M $HClO_4$	$E_{1/2}$ = 0.93 V; SA =2.9 mA cm^{-2}; MA = 0.45 A mg^{-1}	[185]
Pd-P NPs	NaH_2PO_2	Electroless deposition	0.1 M KOH	$E_{1/2}$ = 0.88 V; SA = 6.8 mA cm^{-2} ; MA = 1.34 A mg^{-1}	[179]
HER					
P-Pd_4S NWs	TPS	Liquid-phase synthesis	0.5 M H_2SO_4	η_{10} = 47 mV; Tafel slope = 32.7 mV dec^{-1}; C_{dl}= 2.01 mF cm^{-2}	[186]
P-PtPdCu	TOP	Liquid-phase synthesis	0.5 M H_2SO_4	η_{10} = 12 mV; Tafel slope = 29 mV dec^{-1}; C_{dl}= 1.73 mF cm^{-2}	[187]
Pd_5P_2 @NPGC	$NH_4H_2PO_4$	Gas-solid reaction	1 M KOH	η_{10} = 104 mV	[177]
Pd_5P_2@NC	Phytic acid	Gas-solid reaction	0.5 M H_2SO_4 1 M KOH	η_{10} = 28 mV in 1 M KOH η_{10} = 8 mV in 0.5 M H_2SO_4	[176]
PdP_2@CB	NaH_2PO_2	Gas-solid reaction	1 M KOH 1 M PBS	η_{10} = 35.4 mV, Tafel slope = 42.1 mV dec^{-1} in 1 M KOH η_{10} = 84.6 mV Tafel slope = 72.3 mV dec^{-1} in 1 M PBS	[174]
Pd_3P/NPC	Phytic acid	Gas-solid reaction	0.5 M H_2SO_4 1 M KOH	η_{10} = 277 mV, Tafel slope = 120 mV dec^{-1} in 0.5 M H_2SO_4; η_{10} = 173 mV, Tafel slope = 109 mV dec^{-1} in 1 M KOH	[20]
OER					
PdP_2@CB	NaH_2PO_2	Gas-solid reaction	1 M KOH 1 M PBS	η_{10} = 270 mV, Tafel slope = 78.6 mV dec^{-1} in 1 M KOH; η_{10} = 227 mV, Tafel slope = 96 mV dec^{-1} in 1 M PBS	[174]

dissolution process, and expose more reaction sites, thus facilitating the mass/electron transfer to accelerate the electrocatalytic kinetics. On the other hand, the existence of Cu sites can weaken the adsorption of the intermediates (Co_{ads} and CH_3CO_{ads}) by regulating the electronic state of Pd, and the formation of OH_{ads} on

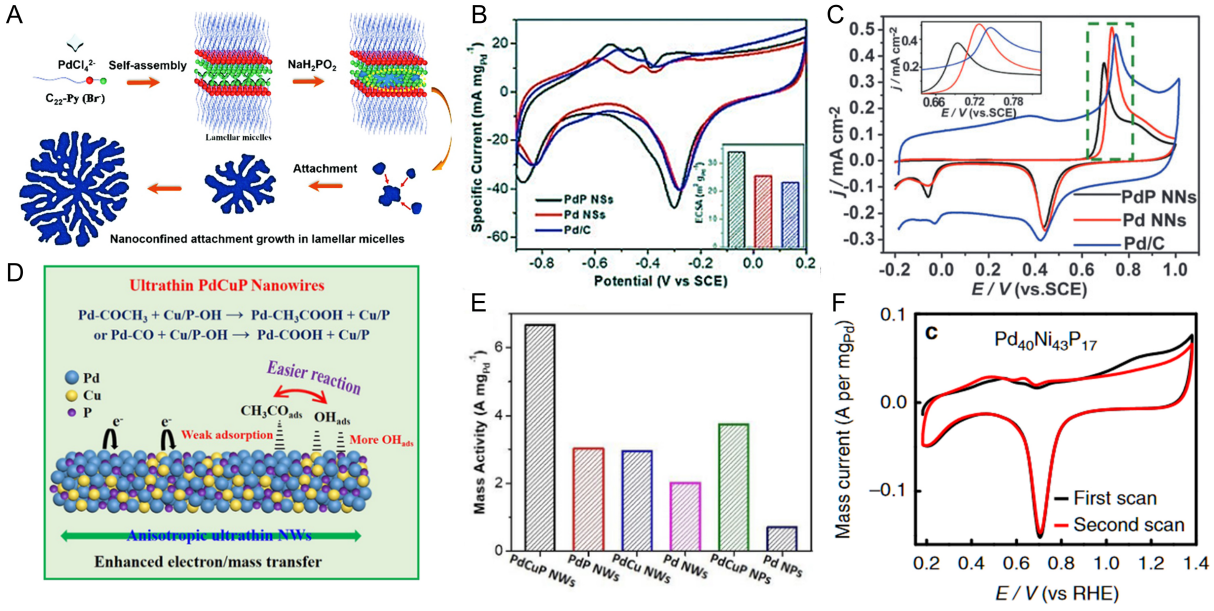

Figure 9. Effect of alloy structures and compositions on the electrocatalytic performance of Pd-based phosphides. (A) Diagram of surfactant-directed aqueous growth of PdP nanosheets; (B) CV curves with insert ESCA diagram of PdP NSs and other counterparts measured in 1.0 M KOH; (A and B) reproduced with permission from[165]: Copyright 2020, The Royal Society of Chemistry; (C) CO stripping curves with insert magnified green square area of PdP nanoparticles and other counterparts. Reproduced with permission from[164]: Copyright 2014, The Royal Society of Chemistry; (D) diagram of ultrathin ternary PdCuP alloy nanowires toward EOR; (E) the difference in mass activities of PdCuP nanowires and their counterparts; (D and E) reproduced with permission from[182]: Copyright 2019, Elsevier; (F) CO stripping curves of $Pd_{40}Ni_{43}P_{17}$ and other counterparts. Reproduced with permission from[169]: Copyright 2017, Nature Publishing Group.

Cu sites can also accelerate the further oxidation of the intermediates to generate acetate ions, which would obviously boost the electrocatalytic kinetics of EOR. Thus, the PdCuP NWs demonstrated the most superior electrocatalytic mass activity with respect to their counterparts [Figure 9E]. This study suggests the key role of P and oxyphilic metal dopants in the improved EOR performance of Pd-based catalysts. However, it is still a tremendous challenge to develop a facile and robust synthetic methodology for the construction of Pd-M-P nanocrystals with advanced nanostructures, ascribed to the complexity or uncertainty in simultaneously achieving the morphological and component control while alloying amorphous P within PdM nanocrystals. By far, only a few efforts paid to the construction of Pd-M-P nanocrystals with advanced nanostructures, such as one-dimensional nanowires[182,184], two-dimensional nanoplates[190], and three-dimensional porous spheres[185]. Besides, in the Pd-M-P nanocrystals, tuning their particle size, surface structure, morphology, and support matrix to enhance their electrocatalytic activity has become a major concern, but less focus on the improved catalytic performance by simultaneously incorporating M/P and shortening the distance between Pd and M active sites. Recently, Chen *et al.*[169] have successful report the enhanced catalytic activity toward EOR of Pd-Ni-P ternary nanocatalysts by tailoring the Ni/Pd atomic ratio to 1:1 and shortening the distance between Pd and Ni active sites [Figure 9F]. It was also found that the activity significantly increased with the decrement of the distance between Pd and Ni active sites. Their research provides a valuable perspective for improving the catalytic activity of P-doped Pd-based catalysts.

More interestingly, many studies have revealed that the activity and stability of P-doped Pd-based nanoalloys can be improved by combining them with conductive supports like graphene[157,173] and carbon[171,178]. For example, PdP nanoalloys with low content phosphorus uniformly embedded in the 3D nitrogen-doped graphene can serve as highly active and stable electrocatalysts for ethanol oxidation reactions in alkaline media[173]. Xie *et al.*[167] designed the PdP_2 nanoparticles to load on rGO, making PdP_2 a

high-performance NRR electrocatalyst for environmental N_2 to NH_3 conversion. Similarly, the palladium nanocatalyst with high-doping phosphorus anchored on the carbon also possesses superior catalytic activity and stability toward FAOR[178]. In a word, these advantages of materials are mainly derived from alloying Pd with P and secondary from the dispersion of active components.

P-doping Pd nanocatalysts are considered to be an effective route to improve the electrocatalytic performance owing to the electronic structure alteration mechanism. Generally, the binding strength of reaction intermediates adsorbed on Pd active sites can be regulated, thereby enhancing the catalytic activities. In this case, a simple and effective synthetic approach that can further regulate the stoichiometry of Pd and P is highly desirable. Even though the PdP and Pd-M-P catalysts have acquired considerable progress, their preparation is still a tremendous challenge. As a result, there is a limitation in the deep understanding of the modification of P-doping. Therefore, it is urgent to develop a precise control preparation of P-doping Pd so that a deeper understanding of the modification of P-doping can be established.

S-doped Pd-based nanocrystals

Pd-based sulfides (Pd_xS_y) have been found to be very important for a variety of electrocatalytic applications due to their special physical-chemical properties[191-193]. The majority of Pd_xS_y can be generally prepared by H_2-assisted gas sulfidation with H_2S[194,195] or by introducing sulfur-containing compounds into an aqueous palladium salt solution[196-198]. In addition, the chemical vapor deposition and the thermal decomposition of organometallic compounds containing Pd-chalcogen bonds into palladium chalcogenides have been developed as another effective strategy to obtain Pd_xS_y[199-201]. However, these methods have suffered from high environmental pollution, high scaling cost, or complicated Pd-chalcogen precursors formation. Recently, Du *et al.* reported a colloidal synthesis of Pd_xS_y (e.g., $Pd_{16}S_7$, Pd_4S, and PdS) *via* a facile one-pot hot-solution synthetic route and applied for the ORR[202]. Such a method can not only reduce the cost and procedures of catalyst preparation but also achieve the controllable component of S in the catalysts by simply tuning the amount of S powder, despite the drawback of high temperature (> 300 °C). Besides, it was found to be readily prepared the supported palladium sulfides through the post-synthetic modification of supported Pd (or oxide) precursors with sulfidation agents such as H_2S, Na_2S and organic sulfur-containing molecules[203-207].

Even though there have been many synthetic approaches reported in the literature for the Pd_xS_y, extremely limited information is available on the factors that determine the phase evolution of Pd-based sulfides and the correlation between the crystal structures and catalytic performances. According to the phase diagram of Pd-S, there are five types of Pd-S crystalline phases, namely PdS, PdS_2, Pd_4S, Pd_3S, and $Pd_{16}S_7$[208]. Since the Pd-S phase diagram shows full mixing in all compositions and a continuum of closely related stable phases, it offers room to tailor the phase evolution of Pd sulfides so that the structure-property relationships can be established[208]. It should be mentioned that phase evolution occurs highly depending on temperature, as observed in the previous reports[209,210]. In this regard, Liu *et al.* have demonstrated how a PdS powder evolves and changes with thermal pre-treatment[211]. The authors found that when the sample was exposed to H_2 at temperatures of 150 °C or higher, the sulfur was lost to the gas phase (H_2S), resulting in the sample undergoing a phase change from a chalcogenide-rich phase (PdS) to a metal-rich phase (Pd_4S) via the $Pd_{16}S_7$ phase as an intermediate. Meanwhile, a new material containing the three phases at the same time would be obtained when the sample is at thermal treatments of 250 °C. Additionally, the sample was almost exclusively converted to the pure Pd_4S phase at thermal treatments of 350 °C. Apart from the temperature, Xu *et al.* prepared a series of Pd_xS_y/C catalysts (Pd_4S, Pd_3S, $Pd_{16}S_7$, and PdS) by tailoring the H_2-assisted sulfidation of Pd/C precursors with H_2S at 150-750 °C, which has proposed that the sulfidation atmosphere, sulfidation temperature, and the metal-support interaction all play important roles in determining the crystal structure and phase evolution of Pd_xS_y/C catalysts[194].

Developing a crystal phase and orientation of controllable Pd-based sulfides is necessary for achieving the desired catalytic performance. Recent works also reveal that the metal-rich Pd_4S phase can be significantly applied in electrocatalytic reactions. As investigated from the DFT calculation by Du *et al.*[202], the existence of oxygen absorption sites in Pd_4S surface can significantly decrease the thermodynamic reaction energy, in which the most and the second most stable configurations at each O coverage hold a huge difference in O adsorption energy [Figure 10A-B]. The adsorption configuration (Pd_4S-$4O_{133}$-O_{112}) was able to trap atomic oxygen moderately and desorb O_2 facilely. This indicates that the stably adsorbed O_{133} sites on the Pd_4S surface contribute to the fast electrode kinetics and facilitate the subsequent adsorption and activation of $*O_2$. Benefiting from the more optimal oxygen adsorption free energy induced by the stably adsorbed O_{133} on the Pd_4S surface, the Pd_4S NPs exhibit superior activity toward ORR with a half-wave potential of 47 mV [Figure 10C].

In addition to the optimized crystal structure, the excellent catalytic performance might also be linked to the interaction between Pd_xS_y nanoparticles and the support. For the supported Pd sulfides with superior catalytic properties, on the one hand, the sulfidation modification could get access to the generation of key structure motifs suitable for the catalytic reactions. This modification might be the combination of a Pd site isolation effect as a result of the crystal phase (Pd_3S or Pd_4S) and a change in the Pd electronic state[207,214]. On the other hand, the formation of strong interaction between guest-host components in the supported Pd sulfides also plays an important role in enhancing the catalytic activity and stability[215]. Based on this, Huang *et al.* reported a S, N-doped carbon-supported Pd_4S catalyst (Pd_4S-SNC) with abundant defects and a hydrangea-like structure for ORR and HER [Figure 10D][212]. Owing to the effective interaction of Pd_4S NPs on the support and the introduction of S dopant in carbon, the aggregation of Pd atoms is largely inhibited, which equips the Pd site with enhanced activity. Moreover, the hydrangea-like structure and the high electronegativity of S and N atoms endow the obtained Pd_4S NPs with numerous active sites and faster reaction kinetics, which can regulate the adsorption-desorption energy of hydrogen or oxygen intermediates to an optimal value, contributing to the improved ORR and HER activity [Figure 10E]. Indeed, when served as HER catalyst, research works have indicated that the decreased free energy of H adsorption induced by the S-edge side might be contributed to the high HER activates[216]. According to the above, these investigations strongly imply the great potential of constructing the supported Pd sulfides with unique crystal phases and Pd_xS_y-support interaction.

Similarly, Wang *et al.* investigated promising partially amorphous PdS nanosheets obtained by sulfuring crystalline Pd NSs for HER to reveal the effect of crystallinity of Pd-based sulfides on the electrocatalytic performance[213]. The HRTEM image shown in Figure 10F reveals that no lattice fringes can be observed in the sulfurized sample, suggesting the crystalline structure has nearly converted into an amorphous structure, as consistent with the XRD patterns. Benefiting from the amorphization transformation and the nanosheet morphology, the partially amorphous PdS NSs exhibit more excellent HER activity than their crystalline counterparts [Figure 10G]. This investigation strongly implies the enormous potential of constructing Pd-based sulfides with unique crystal phases, crystallinity, and Pd_xS_y-support interaction.

Multi-nonmetals doped Pd-based nanocrystals

It is well accepted that the favorable introduction of nonmetallic elements into Pd-based nanostructures enables catalysts with significantly improved catalytic performance over pure metal Pd catalysts. Recently, some works have highlighted that dual-nonmetals doping could bring about more significant improvement due to the synergistic effects between the heteroatoms compared with single nonmetal-doping

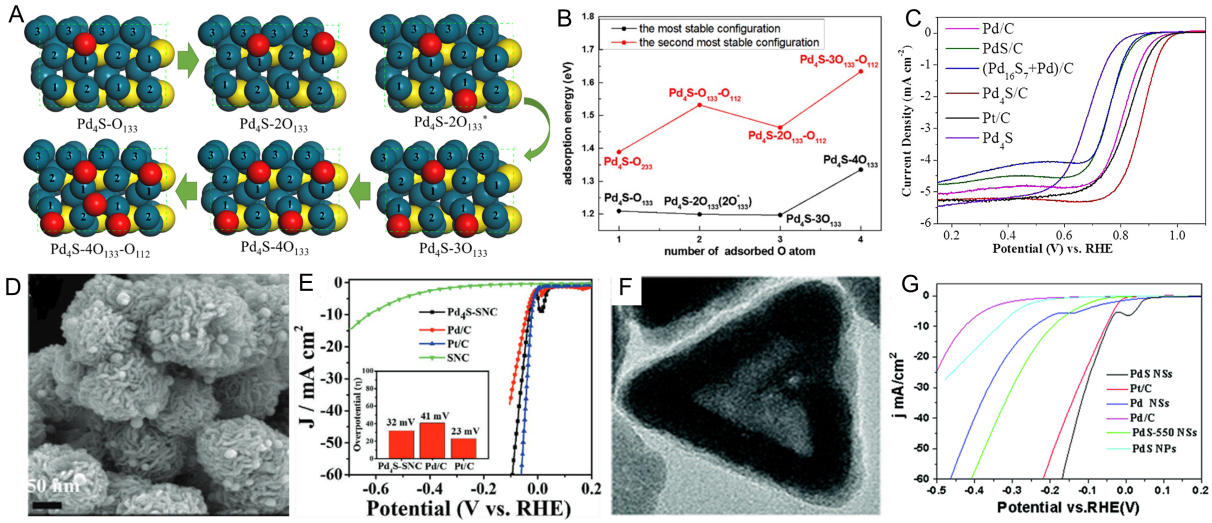

Figure 10. Effect of the crystal structure and modified supports on the electrocatalytic performance of Pd-based sulfides. (A) Different adsorption configurations of reaction intermediates on metal-rich Pd_4S (110) phase; (B) O adsorption energies of the most stable adsorption configurations and the sub-stable adsorption configurations at different O coverages; (C) LSV curves of the Pd_4S and other reference catalysts in 0.1 M KOH; (A-C) reproduced with permission from[202]: Copyright 2018, American Chemical Society; (D) SEM images of Pd_4S-SNC and (E) HER polarization curves of Pd_4S-SNC and reference catalysts in 0.5 M H_2SO_4 solution; (D and E) reproduced with permission from[212]: Copyright 2021, Wiley-VCH; (F) HRTEM of the PdS NSs and corresponding (G) LSV curves; (F and G) reproduced with permission from[213]: Copyright 2021, The Royal Society of Chemistry.

counterparts[217,218]. For example, Yin *et al.* reported the S and P-co-doped mesoporous PtPd nanocages (PtPdSP mNCs) as efficient acidic ORR electrocatalysts[219]. According to theoretical results, S and P-co-doping result in a large number of low-coordinate active sites on the Pd surface, the synergetic electronic interactions between the metal and nonmetal elements, and the lattice expansion of metals. Interestingly, the two former results cause the downshift of the *d*-band center of Pd, while the latter has the opposite effect. The authors claimed that the modification of electronic structures and a downshift of the d-band center position could weaken the bond energy between the Pt surface and the adsorbed species, thus making a substantial contribution to the excellent intrinsic ORR activity. Xu *et al.* also found that the co-doping of B and P tuned the electronic and geometric structures of Pd atoms, leading to a superior FAOR performance[220]. In their study, the B, P-co-doping PdRu nanospine assemblies were found to form oxygen-containing species (e.g., Ru-OH_{ads}, BO_x, and PO_x) that could facilitate the oxidation of the adsorbed oxygen species at a low potential. As confirmed by electrochemical measurements, the as-fabricated PdRuBP had a high specific activity (4.51 mA $cm^{-2)}$ and a mass activity (1.71 mA μg_{Pd}^{-1}), likely because of a weakened bonding between the Pd surface and adsorbed oxygenated species.

From the viewpoint of geometric structure, the co-incorporation of dual-type nonmetallic atoms brings about not only lattice expansion, but also a way to some extent enhance performance through constructing heterointerface. A recent revisit of the reported $Pd_4S/Pd_3P_{0.95}$ heterostructure has identified the presence of abundant Pd_4S and Pd_3P phases[221]. The authors emphasized the heterostructure could significantly promote the HER reaction kinetic. On the one hand, the $Pd_4S/Pd_3P_{0.95}$ heterostructure has a much lower R_{ct} value (4.3 Ω) relative to Pd_4S (28.5 Ω) and $Pd_3P_{0.95}$ (40 Ω), indicating that the greatly enhanced charge transfer capacity. In other words, the presence of $Pd_4S/Pd_3P_{0.95}$ heterointerface helps to reduce the number of formed oxidation species, leading to the strong surface antioxidative ability. DFT also confirmed that the $Pd_4S/Pd_3P_{0.95}$ has a weaker water dissociation energy barrier (1.04 eV) than Pd_4S (1.29 eV) and $Pd_3P_{0.95}$ (1.24 eV). These results demonstrated the ability of heterointerface to regulate the activity and durability of alkaline HER and encouraged the study of constructing multi-nonmetal doping Pd-based heterostructures.

CONCLUSION AND OUTLOOK

With decades of development, metal-nonmetal nanocrystals play important roles in electrocatalysis, and the modification of Pd metal with various nonmetals has stood out as one of the most effective strategies for searching for suitable Pt-free catalysts. Growing attention has been implemented to modulate nonmetal elements in noble metals. In this review, we have reviewed the recent progress in nonmetal element-doped Pd nanocrystals, including Pd-based hydrides, borides, carbides, nitrides, oxides, phosphides, and sulfides, as well as their electrocatalytic applications. These doped elements into palladium, which are recognized as ideal promoters for various electrocatalytic reactions, offer a positive role in optimizing the atomic structure, electronic properties, and surface adsorption behavior, thereby achieving excellent catalytic activity, stability, and selectivity.

Although great progress has been made in the development of Pd-nonmetal nanocrystals, several major challenges to the development of highly efficient and stable Pd-nonmetal based catalysts still exist in academic research and industrial production. To further promote the synthesis and catalytic application of such catalysts, a shortlist of these challenges and the potential directions for future studies has been proposed.

(i) There is still a lack of more accurate and controllable strategies for preparing Pd-nonmetal nanocrystals with well-designed morphologies, phases, and compositions. It is well known that catalyst nanostructure optimization with precisely controlled morphologies and composition plays a decisive role in determining the electrocatalytic efficiency of nanomaterials. However, the preparation of Pd-nonmetal nanocrystals often depends on elevated temperature/pressure reaction conditions, leading to uncontrolled crystallization processes and large-grain production, which limit the ability to design well-designed morphologies and compositions. Generally, these parameters will change the electronic structure and the surface adsorption behavior of the obtained Pd-nonmetal nanocrystals, resulting in a considerable influence on catalytic performance. Therefore, mild synthesis approaches should be urgently developed. Especially for nonmetallic atoms with relatively smaller atomic radius (e.g., H and B), their existence in Pd lattices is often random and structurally unstable, which restrict their electrocatalytic applications. It should be noted that the doping amount, type, and location in Pd also have a significant impact on the final product. Therefore, developing simple strategies for introducing stable nonmetal elements and controlling the amount, type, and location are required. In addition, the doping of those elements (e.g., B, C, and S) can form structurally ordered intermetallic, which usually tend to produce a mixed phase with different stoichiometric ratios based on the fixed constituent element. Hence, it is also necessary to develop and synthesize pure-phase intermetallics and prepare them for practical applications.

(ii) There is a lack of in-depth mechanistic studies on the role of doping modification of nonmetal elements. The nonmetallic heteroatoms (e.g., H, B, C, N, O, P, and S) doping in the Pd nanostructure offers multiple effects simultaneously, such as a lattice expansion, phase evolution, charge redistribution, and orbital hybridization coupling, to institute the new electrochemical active sites, thus effectively regulating the adsorption energy of the reactants at the active sites which ultimately lead to the enhanced activity. Obviously, rational elucidation of the correlation between catalytic activity and each doping effect plays an important role in providing theoretical guidance for the rational design and construction of Pd-nonmetal nanocrystals. From the fundamental point of view, although more and more such catalysts have been reported to show much improved catalytic performance, little work was done on simultaneously discussing the multiple effects. Therefore, mechanistic studies based on considering all doping effects are crucial. In addition, the nonmetallic heteroatoms in Pd may undergo dynamic evolution; thus, conventional experiments and *ex-suit* characterization may not reflect or even provide misleading information due to the

unstable intermediate species and possible air exposure. Hence, we believe that a combination of theoretical and experimental strategies, together with the *in-situ* characterization techniques, will improve the fundamental understanding of the mechanism of doping modification of nonmetal elements.

(iii) The stability of the single nonmetal doped Pd-based nanocrystals is limited. On the one hand, as aforementioned, the nonmetallic heteroatoms in Pd lattices may undergo dynamic evolution, such as oxidation or migration under harsh operation conditions (e.g., high temperature, high pressured extreme pH environment), resulting in a compromise between intrinsic activity and stability. On the other hand, the activity can also be gradually lost with the corrosion of Pd sites in acidic or alkaline media, leading to poor durability. To end this, the Pd metal can be alloyed with secondary metals M (e.g., Rh,[42,47] Mo,[44,222] Ni,[134,168,169,181,183] and Cu[81,82,130,182]) while incorporating the nonmetallic heteroatoms NM to form the Pd-M-NM structures, which have been demonstrated as an effective promoter for the catalytic stability. Moreover, the together introduction of multiple nonmetallic heteroatoms into Pd-based catalysts, such as PdBP[218,223] and PdBS[224], has also been reported to become a promising strategy for improving catalytic stability. Considering this, developing facile and robust methods to fabricate multi-nonmetallic doped Pd materials with alloying secondary metals to find novel high-performance catalysts is a promising research direction.

In summary, developing nonmetal-doped Pd-based electrocatalysts in different energy-related electrocatalytic applications is very promising but still challenging. Given the large family of nonmetal doped Pd-based catalysts available regarding composition and their unique physical/chemical properties, more studies on these catalysts need to be performed. With the continuing research efforts, it is believed that such materials would provide a considerable incentive for further electrochemical energy conversion investigation.

DECLARATIONS

Acknowledgments

The authors are grateful for the support from National and Local Joint Engineering Research Center of Biomedical Functional Materials and a project sponsored by the Priority Academic Program Development of Jiangsu Higher Education Institutions.

Authors' contributions

Prepared and revised the manuscript: Wang C, Wang Y
Revised the manuscript: Jiang X, Zhou J
Designed and revised the manuscript: Fu G, Tang Y
All authors contributed to the discussion and preparation of the manuscript.

Availability of data and materials

Not applicable.

Financial support and sponsorship

This work was financially supported by the National Natural Science Foundation of China (22232004, 22279062 and 22202104), the Natural Science Foundation of Jiangsu Province (BK20220933), Shuangchuang Doctor Plan of Jiangsu Province, Jiangsu Specially Appointed Professor Plan, and Science and Technology Innovation Project for Overseas Researchers in Nanjing. The authors are grateful for the support from National and Local Joint Engineering Research Center of Biomedical Functional Materials and a project sponsored by the Priority Academic Program Development of Jiangsu Higher Education Institutions.

Conflicts of interest

All authors declared that there are no conflicts of interest.

Ethical approval and consent to participate

Not applicable.

Consent for publication

Not applicable.

REFERENCES

1. Nitopi S, Bertheussen E, Scott SB, et al. Progress and perspectives of electrochemical CO_2 reduction on copper in aqueous electrolyte. *Chem Rev* 2019;119:7610-72. DOI
2. Chu S, Cui Y, Liu N. The path towards sustainable energy. *Nat Mater* 2016;16:16-22. DOI
3. Seh ZW, Kibsgaard J, Dickens CF, et al. Combining theory and experiment in electrocatalysis: Insights into materials design. *Science* 2017;355:eaad4998. DOI
4. Li Z, Wu X, Jiang X, et al. Surface carbon layer controllable Ni_3Fe particles confined in hierarchical N-doped carbon framework boosting oxygen evolution reaction. *Adv Powder Mater* 2022;1:100020. DOI
5. Li Y, Yu H, Wang Z, et al. Boron-doped silver nanosponges with enhanced performance towards electrocatalytic nitrogen reduction to ammonia. *Chem Commun* 2019;55:14745-8. DOI
6. Zhao R, Chen Z, Li Q, et al. N-doped $LaPO_4$: an effective Pt-free catalyst for electrocatalytic oxygen reduction. *Chem Catal* 2022;2:3590-606. DOI
7. Hu S-N, Tian N, Li M-Y, et al. Trapezohedral platinum nanocrystals with high-index facets for high-performance hydrazine electrooxidation. *Chem Synth* 2023;3:4. DOI
8. Wang X, Wang J, Wang P, et al. Engineering 3d-2p-4f gradient orbital coupling to enhance electrocatalytic oxygen reduction. *Adv Mater* 2022;34:2206540. DOI
9. Wang W, Li X, He T, Liu Y, Jin M. Engineering surface structure of Pt nanoshells on Pd nanocubes to preferentially expose active surfaces for ORR by manipulating the growth kinetics. *Nano Lett* 2019;19:1743-8. DOI
10. Li Y, Peng C-K, Hu H, et al. Interstitial boron-triggered electron-deficient Os aerogels for enhanced pH-universal hydrogen evolution. *Nat Commun* 2022;13:1143. DOI
11. Li Q, Wang X, Xie Z, et al. Polar bonds induced strong Pd-support electronic interaction drives remarkably enhanced oxygen reduction activity and stability. *Appl Catal B* 2022;305:121020. DOI
12. Jiang X, Xiong Y, Wang Y, et al. Treelike two-level Pd_xAg_y nanocrystals tailored for bifunctional fuel cell electrocatalysis. *J Mater Chem A* 2019;7:5248-57. DOI
13. Jiang X, Wang J, Huang T, et al. Sub-5 nm palladium nanoparticles in situ embedded in N-doped carbon nanoframes: facile synthesis, excellent sinter resistance and electrocatalytic properties. *J Mater Chem A* 2019;7:26243-9. DOI
14. Yang Y, Zhu X, Wang L, et al. Breaking scaling relationships in alkynol semi-hydrogenation by manipulating interstitial atoms in Pd with d-electron gain. *Nat Commun* 2022;13:2754. DOI
15. Su L, Zhao Y, Jin Y, et al. Identifying the role of hydroxyl binding energy in a non-monotonous behavior of Pd-Pd_4S for hydrogen oxidation reaction. *Adv Funct Mater* 2022;32:2113047. DOI
16. Wang N, Zhao X, Zhang R, et al. Highly selective oxygen reduction to hydrogen peroxide on a carbon-supported single-atom Pd electrocatalyst. *ACS Catal* 2022;12:4156-64. DOI
17. Liu H, Fu J, Li H, et al. Single palladium site in ordered porous heteroatom-doped carbon for high-performance alkaline hydrogen oxidation. *Appl Catal B* 2022;306:121029. DOI
18. Lee S J, Theerthagiri J, Nithyadharseni P, et al. Heteroatom-doped graphene-based materials for sustainable energy applications: a review. *Renew Sustain Energy Rev* 2021;143:110849. DOI
19. Dann EK, Gibson EK, Blackmore RH, et al. Structural selectivity of supported Pd nanoparticles for catalytic NH_3 oxidation resolved using combined operando spectroscopy. *Nat Catal* 2019;2:157-63. DOI
20. Qin Q, Jang H, Chen L, et al. Coupling a low loading of IrP_2, PtP_2, or Pd_3P with heteroatom-doped nanocarbon for overall water-splitting cells and zinc-air batteries. *ACS Appl Mater Interf* 2019;11:16461-73. DOI
21. Jiang TW, Zhou YW, Ma XY, et al. Spectrometric study of electrochemical CO_2 reduction on Pd and Pd-B electrodes. *ACS Catal* 2021;11:840-8. DOI
22. Wang YF, Zhu C, Yang YY, Zhao ZG. Surface-clean low-doped PdB/C as superior electrocatalysts toward ethanol oxidation in alkaline media. *J Energy Chem* 2018;27:389-94. DOI

23. Vo Doan TT, Wang J, Poon KC, et al. Theoretical modelling and facile synthesis of a highly active boron-doped palladium catalyst for the oxygen reduction reaction. *Angew Chem Int Ed* 2016;55:6842-7. DOI
24. Chan C WA, Mahadi A H, Li M M-J, et al. Interstitial modification of palladium nanoparticles with boron atoms as a green catalyst for selective hydrogenation. *Nat Commun* 2014;5:5787. DOI
25. Chen H, Zhang B, Liang X, Zou X. Light alloying element-regulated noble metal catalysts for energy-related applications. *Chinese J Catal* 2022;43:611-35. DOI
26. Wang M, Li L, Wang M, Huang X. Recent progress in palladium-nonmetal nanostructure development for fuel cell applications. *NPG Asia Mater* 2022;14:1-8. DOI
27. Zhang C, Liu W, Chen C, et al. Emerging interstitial/substitutional modification of Pd-based nanomaterials with nonmetallic elements for electrocatalytic applications. *Nanoscale* 2022;14:2915-42. DOI
28. Guo R, Zhang K, Ji S, Zheng Y, Jin M. Recent advances in nonmetallic atom-doped metal nanocrystals: synthesis and catalytic applications. *Chin Chem Lett* 2021;32:2679-92. DOI
29. Wang S, Tian D, Wang X, et al. Uniform $PdH_{0.33}$ nanodendrites with a high oxygen reduction activity tuned by lattice H. *Electrochem Commun* 2019;102:67-71. DOI
30. Kim D, Koh J, Kang S, et al. Chemomechanical effect of reduced graphene oxide encapsulation on hydrogen storage performance of Pd nanoparticles. *J Mater Chem A* 2021;9:11641-50. DOI
31. Liu Y, Chen Z, Liu C, et al. Exploiting H-induced lattice expansion in *β*-palladium hydride for enhanced catalytic activities toward oxygen reduction reaction. *J Mater Sci Technol* 2022;98:205-11. DOI
32. Xu W, Fan G, Chen J, et al. Nanoporous palladium hydride for electrocatalytic N_2 reduction under ambient conditions. *Angew Chem Int Ed Engl* 2020;59:3511-6. DOI
33. Zhu Y, Gao C, Bai S, et al. Hydriding Pd cocatalysts: an approach to giant enhancement on photocatalytic CO_2 reduction into CH_4. *Nano Res* 2017;10:3396-406. DOI
34. Wang Z, Dai Z, Wang S, et al. Enhancing electrochemical ammonia synthesis on palladium nanorods through surface hydrogenation. *Chem Eng J* 2021;416:129105. DOI
35. Liu G, Zhou W, Ji Y, et al. Hydrogen-intercalation-induced lattice expansion of Pd@Pt core-shell nanoparticles for highly efficient electrocatalytic alcohol oxidation. *J Am Chem Soc* 2021;143:11262-70. DOI
36. Zhao P, Jin Z, Chen Q, et al. Local generation of hydrogen for enhanced photothermal therapy. *Nat Commun* 2018;9:4241. DOI
37. Shi Y, Schimmenti R, Zhu S, et al. Solution-phase synthesis of $PdH_{0.706}$ nanocubes with enhanced stability and activity toward formic acid oxidation. *J Am Chem Soc* 2022;144:2556-68. DOI
38. Lin B, Wu X, Xie L, et al. Atomic imaging of subsurface interstitial hydrogen and insights into surface reactivity of palladium hydrides. *Angew Chem Int Ed* 2020;59:20348-52. DOI
39. Rahul R, Singh RK, Bera B, Devivaraprasad R, Neergat M. The role of surface oxygenated-species and adsorbed hydrogen in the oxygen reduction reaction (ORR) mechanism and product selectivity on Pd-based catalysts in acid media. *Phys Chem Chem Phys* 2015;17:15146-55. DOI
40. Zhan C, Li H, Li X, Jiang Y, Xie Z. Synthesis of $PdH_{0.43}$ nanocrystals with different surface structures and their catalytic activities towards formic acid electro-oxidation. *Sci China Mater* 2019;63:375-82. DOI
41. Wang D, Jiang X, Lin Z, et al. Ethanol-induced hydrogen insertion in ultrafine IrPdH boosts pH-universal hydrogen evolution. *Small* 2022;18:2204063. DOI
42. Fan J, Wu J, Cui X, et al. Hydrogen stabilized RhPdH 2D bimetallene nanosheets for efficient alkaline hydrogen evolution. *J Am Chem Soc* 2020;142:3645-51. DOI
43. Zhao Z, Flores Espinosa M M, Zhou J, et al. Synthesis of surface controlled nickel/palladium hydride nanodendrites with high performance in benzyl alcohol oxidation. *Nano Res* 2019;12:1467-72. DOI
44. Wu J, Cui X, Fan J, et al. Stable bimetallene hydride boosts anodic CO tolerance of fuel cells. *ACS Energy Lett* 2021;6:1912-9. DOI
45. Lu Y, Wang J, Peng Y, Fisher A, Wang X. Highly efficient and durable Pd hydride nanocubes embedded in 2D amorphous NiB nanosheets for oxygen reduction reaction. *Adv Energy Mater* 2017;7:1700919. DOI
46. Bu L, Zhu X, Zhu Y, et al. H-implanted Pd icosahedra for oxygen reduction catalysis: from calculation to practice. *CCS Chem* 2021;3:1972-82. DOI
47. Fan J, Cui X, Yu S, et al. Interstitial hydrogen atom modulation to boost hydrogen evolution in Pd-based alloy nanoparticles. *ACS Nano* 2019;13:12987-95. DOI
48. Sun H Y, Ding Y, Yue Y Q, et al. Bifunctional palladium hydride nanodendrite electrocatalysts for hydrogen evolution integrated with formate oxidation. *ACS Appl Mater Interf* 2021;13:13149-57. DOI
49. Jia Y, Huang T-H, Lin S, et al. Stable Pd–Cu hydride catalyst for efficient hydrogen evolution. *Nano Lett* 2022;22:1391-7. DOI
50. Zhao Z, Huang X, Li M, et al. Synthesis of stable shape-controlled catalytically active β-palladium hydride. *J Am Chem Soc* 2015;137:15672-5. DOI
51. Guo X, Hu Z, Lv J, Qu J, Hu S. Palladium hydride with high-index facets for enhanced methanol oxidation. *Dalton Trans* 2021;50:10359-64. DOI
52. Kabiraz M K, Kim J, Lee W-J, et al. Ligand effect of shape-controlled β-palladium hydride nanocrystals on liquid-fuel oxidation reactions. *Chem Mater* 2019;31:5663-73. DOI
53. Zhang J, Chen M, Li H, et al. Stable palladium hydride as a superior anode electrocatalyst for direct formic acid fuel cells. *Nano*

Energy 2018;44:127-34. DOI
54. Chang Q, Kim J, Lee J H, et al. Boosting activity and selectivity of CO_2 electroreduction by pre-hydridizing Pd nanocubes. *Small* 2020;16:2005305. DOI
55. Baldi A, Narayan T C, Koh A L, Dionne J A. In situ detection of hydrogen-induced phase transitions in individual palladium nanocrystals. *Nat Mater* 2014;13:1143-8. DOI
56. Li G, Kobayashi H, Taylor J M, et al. Hydrogen storage in Pd nanocrystals covered with a metal-organic framework. *Nat Mater* 2014;13:802-6. DOI
57. Pei Y, Zhou G, Luan N, et al. Synthesis and catalysis of chemically reduced metal–metalloid amorphous alloys. *Chem Soc Rev* 2012;41:8140-62. DOI
58. Carenco S, Portehault D, Boissière C, Mézailles N, Sanchez C. Nanoscaled metal borides and phosphides: recent developments and perspectives. *Chem Rev* 2013;113:7981-8065. DOI
59. Wang G, Liu J, Sui Y, et al. Palladium structure engineering induced by electrochemical H intercalation boosts hydrogen evolution catalysis. *J Mater Chem A* 2019;7:14876-81. DOI
60. Chen T, Chen S, Song P, et al. Single-molecule nanocatalysis reveals facet-dependent catalytic kinetics and dynamics of pallidium nanoparticles. *ACS Catal* 2017;7:2967-72. DOI
61. Li G, Kobayashi H, Dekura S, et al. Shape-dependent hydrogen-storage properties in Pd nanocrystals: which does hydrogen prefer, octahedron (111) or cube (100)? *J Am Chem Soc* 2014;136:10222-5. DOI
62. Yang H G, Sun C H, Qiao S Z, et al. Anatase TiO_2 single crystals with a large percentage of reactive facets. *Nature* 2008;453:638-41. DOI
63. Koper M T M. Structure sensitivity and nanoscale effects in electrocatalysis. *Nanoscale* 2011;3:2054-73. DOI
64. Kondo S, Nakamura M, Maki N, Hoshi N. Active sites for the oxygen reduction reaction on the low and high index planes of palladium. *J Phys Chem C* 2009;113:12625-8. DOI
65. Erikson H, Sarapuu A, Alexeyeva N, et al. Electrochemical reduction of oxygen on palladium nanocubes in acid and alkaline solutions. *Electrochim Acta* 2012;59:329-35. DOI
66. Erikson H, Sarapuu A, Tammeveski K, Solla-Gullón J, Feliu J M. Enhanced electrocatalytic activity of cubic Pd nanoparticles towards the oxygen reduction reaction in acid media. *Electrochem Commun* 2011;13:734-7. DOI
67. Zhu W, Kattel S, Jiao F, Chen J G. Shape-controlled CO_2 electrochemical reduction on nanosized Pd hydride cubes and octahedra. *Adv Energy Mater* 2019;9:1802840. DOI
68. Johnson NJJ, Lam B, Sherbo RS, Fork DK, Berlinguette CP. Ligands affect hydrogen absorption and desorption by palladium nanoparticles. *Chem Mater* 2019;31:8679-84. DOI
69. Kitchin JR, Norskov JK, Barteau MA, Chen JG. Role of strain and ligand effects in the modification of the electronic and chemical properties of bimetallic surfaces. *Phys Rev Lett* 2004;93:156801. DOI
70. Moseley P, Curtin WA. Computational design of strain in core-shell nanoparticles for optimizing catalytic activity. *Nano Lett* 2015;15:4089-95. DOI
71. Wang L, Zeng Z, Gao W, et al. Tunable intrinsic strain in two-dimensional transition metal electrocatalysts. *Science* 2019;363:870-4. DOI
72. Kobayashi K, Kobayashi H, Maesato M, et al. Discovery of hexagonal structured Pd-B nanocrystals. *Angew Chem Int Ed* 2017;56:6578-82. DOI
73. Lu W, Liu T, Xie L, et al. In situ derived Co-B nanoarray: a high-efficiency and durable 3D bifunctional electrocatalyst for overall alkaline water splitting. *Small* 2017;13:1700805. DOI
74. Masa J, Sinev I, Mistry H, et al. Ultrathin high surface area nickel boride (Ni_xB) nanosheets as highly efficient electrocatalyst for oxygen evolution. *Adv Energy Mater* 2017;7:1700381. DOI
75. Regmi YN, Mann JK, McBride JR, et al. Catalytic transfer hydrogenolysis of organosolv lignin using B-containing FeNi alloyed catalysts. *Catal Today* 2018;302:190-5. DOI
76. Wang M, Qin X, Jiang K, et al. Electrocatalytic activities of oxygen reduction reaction on Pd/C and Pd-B/C catalysts. *J Phys Chem C* 2017;121:3416-23. DOI
77. Li H, Qin X, Zhang XG, Jiang K, Cai WB. Boron-doped platinum-group metals in electrocatalysis: a perspective. *ACS Catal* 2022;12:12750-64. DOI
78. Wang JY, Kang YY, Yang H, Cai WB. Boron-doped palladium nanoparticles on carbon black as a superior catalyst for formic acid electro-oxidation. *J Phys Chem C* 2009;113:8366-72. DOI
79. Ellis IT, Wolf EH, Jones G, et al. Lithium and boron as interstitial palladium dopants for catalytic partial hydrogenation of acetylene. *Chem Commun* 2017;53:601-4. DOI
80. Yoo JS, Zhao ZJ, Nørskov JK, Studt F. Effect of boron modifications of palladium catalysts for the production of hydrogen from formic acid. *ACS Catal* 2015;5:6579-86. DOI
81. Wang Y, Lv H, Sun L, et al. Ultrathin and wavy PdB alloy nanowires with controlled surface defects for enhanced ethanol oxidation electrocatalysis. *ACS Appl Mater Interf* 2021;13:17599-607. DOI
82. Sun L, Lv H, Wang Y, Xu D, Liu B. Unveiling synergistic effects of interstitial boron in palladium-based nanocatalysts for ethanol oxidation electrocatalysis. *J Phys Chem Lett* 2020;11:6632-9. DOI
83. Lv H, Sun L, Xu D, et al. Mesoporous palladium–boron alloy nanospheres. *J Mater Chem A* 2019;7:24877-83. DOI

84. Li J, Chen J, Wang Q, Cai WB, Chen S. Controllable increase of boron content in B-Pd interstitial nanoalloy to boost the oxygen reduction activity of palladium. *Chem Mater* 2017;29:10060-7. DOI
85. Hong S, Chung S, Park J, et al. Contribution of interstitial boron in a boron-incorporated palladium catalyst toward formate oxidation in an alkaline direct formate fuel cell. *ACS Catal* 2021;11:4722-9. DOI
86. Jiang B, Zhang XG, Jiang K, Wu DY, Cai WB. Boosting formate production in electrocatalytic CO_2 reduction over wide potential window on Pd surfaces. *J Am Chem Soc* 2018;140:2880-9. DOI
87. Wang Q, Liao Y, Zhang H, et al. One-pot synthesis of carbon-supported monodisperse palladium nanoparticles as excellent electrocatalyst for ethanol and formic acid oxidation. *J Power Sources* 2015;292:72-7. DOI
88. Lv H, Xu D, Kong C, et al. Synthesis and crystal-phase engineering of mesoporous palladium-boron alloy nanoparticles. *ACS Cent Sci* 2020;6:2347-53. DOI
89. Li Z, Xie Z, Chen H, et al. Realization of interstitial boron ordering and optimal near-surface electronic structure in Pd-B alloy electrocatalysts. *Chem Eng J* 2021;419:129568. DOI
90. Jiang K, Chang J, Wang H, et al. Small addition of boron in palladium catalyst, big improvement in fuel cell's performance: what may interfacial spectroelectrochemistry tell? *ACS Appl Mater Interf* 2016;8:7133-8. DOI
91. Ai X, Zou X, Chen H, et al. Transition-metal-boron intermetallics with strong interatomic *d-sp* orbital hybridization for high-performance electrocatalysis. *D-sp* ;59:3961-5. DOI
92. Teschner D, Borsodi J, Wootsch A, et al. The roles of subsurface carbon and hydrogen in palladium-catalyzed alkyne hydrogenation. *Science* 2008;320:86-9. DOI
93. Ziemecki SB, Jones GA, Swartzfager DG, Harlow RL, Faber J. Formation of interstitial palladium-carbon phase by interaction of ethylene, acetylene, and carbon monoxide with palladium. *J Am Chem Soc* 1985;107:4547-8. DOI
94. Maciejewski M, Baiker A. Incorporation of carbon into palladium during low-temperature disproportionation of carbon monoxide over palladium/zirconia prepared from glassy palladium-zirconium. *J Phys Chem* 1994;98:285-90. DOI
95. Zaidi AH. Stability of Pd-C phase in the oxidation of ethylene over palladium catalysts. *Appl Catal* 1987;30:131-40. DOI
96. Wang C, Jia Y, Zhang Z, et al. Role of PdC_x species in $Pd@PdC_x$/AlOOH/Al-fiber catalyst for the CO oxidative coupling to dimethyl oxalate. *Appl Surf Sci* 2019;478:840-5. DOI
97. Simonov AN, Pyrjaev PA, Simonov PA, et al. Enhanced catalytic activity for hydrogen electrooxidation and CO tolerance of carbon-supported non-stoichiometric palladium carbides. *J Mol Catal A Chem* 2012;353-354:204-14. DOI
98. Teschner D, Révay Z, Borsodi J, et al. Understanding palladium hydrogenation catalysts: when the nature of the reactive molecule controls the nature of the catalyst active phase. *Angew Chem Int Ed* 2008;47:9274-8. DOI
99. Brandt B, Fischer JH, Ludwig W, et al. Isomerization and hydrogenation of cis-2-butene on Pd model catalyst. *J Phys Chem C* 2008;112:11408-20. DOI
100. Huang F, Jia Z, Diao J, et al. Palladium nanoclusters immobilized on defective nanodiamond-graphene core-shell supports for semihydrogenation of phenylacetylene. *J Energy Chem* 2019;33:31-6. DOI
101. Shao L, Zhang B, Zhang W, et al. Improved selectivity by stabilizing and exposing active phases on supported Pd nanoparticles in acetylene-selective hydrogenation. *Chem Eur J* 2012;18:14962-6. DOI
102. Canton P, Meneghini C, Riello P, Balerna A, Benedetti A. Thermal evolution of carbon-supported Pd nanoparticles studied by time-resolved X-ray diffraction. *J Phys Chem B* 2001;105:8088-91. DOI
103. Makkee M, van de Sandt EJAX, Wiersma A, Moulijn JA. Development of a satisfactory palladium on activated carbon catalyst for the selective hydrogenolysis of CCl_2F_2(CFC-12) into CH_2F_2(HFC-32). *J Mol Catal A Chem* 1998;134:191-200. DOI
104. Wakisaka T, Kusada K, Wu D, et al. Rational synthesis for a noble metal carbide. *J Am Chem Soc* 2020;142:1247-53. DOI
105. Okitsu K, Mizukoshi Y, Bandow H, et al. Synthesis of palladium nanoparticles with interstitial carbon by sonochemical reduction of tetrachloropalladate(II) in aqueous solution. *J Phys Chem B* 1997;101:5470-2. DOI
106. Guo R, Chen Q, Li X, et al. PdC_x nanocrystals with tunable compositions for alkyne semihydrogenation. *J Mater Chem A* 2019;7:4714-20. DOI
107. Garcia-Ortiz A, Vidal J D, Iborra S, et al. Synthesis of a hybrid Pd_0/Pd-carbide/carbon catalyst material with high selectivity for hydrogenation reactions. *J Catal* 2020;389:706-13. DOI
108. Piqué O, Koleva IZ, Viñes F, et al. Subsurface carbon: a general feature of noble metals. *Angew Chem Int Ed* 2019;58:1744-8. DOI
109. Lord RW, Holder CF, Fenton JL, Schaak RE. Seeded growth of metal nitrides on noble-metal nanoparticles to form complex nanoscale heterostructures. *Chem Mater* 2019;31:4605-13. DOI
110. Gage SH, Trewyn BG, Ciobanu CV, Pylypenko S, Richards RM. Synthetic advancements and catalytic applications of nickel nitride. *Catal Sci Technol* 2016;6:4059-76. DOI
111. Alexander AM, Hargreaves JSJ. Alternative catalytic materials: carbides, nitrides, phosphides and amorphous boron alloys. *Chem Soc Rev* 2010;39:4388-401. DOI
112. Marchand R, Laurent Y, Guyader J, L'Haridon P, Verdier P. Nitrides and oxynitrides: preparation, crystal chemistry and properties. *J Eur Ceram Soc* 1991;8:197-213. DOI
113. Miura A, Lowe M, Leonard BM, et al. Silver delafossite nitride, $AgTaN_2$? *J Solid State Chem* 2011;184:7-11. DOI
114. Balogun MS, Zeng Y, Qiu W, et al. Three-dimensional nickel nitride (Ni_3N) nanosheets: free standing and flexible electrodes for lithium ion batteries and supercapacitors. *J Mater Chem A* 2016;4:9844-9. DOI
115. Lu X, Liu T, Zhai T, et al. Improving the cycling stability of metal-nitride supercapacitor electrodes with a thin carbon shell. *Adv*

Energy Mater 2014;4:1300994. DOI
116. Lu X, Wang G, Zhai T, et al. Stabilized TiN nanowire arrays for high-performance and flexible supercapacitors. *Nano Lett* 2012;12:5376-81. DOI
117. Meng F, Zhong H, Bao D, Yan J, Zhang X. In situ coupling of strung Co_4N and intertwined N-C fibers toward free-standing bifunctional cathode for robust, efficient, and flexible Zn-air batteries. *J Am Chem Soc* 2016;138:10226-31. DOI
118. Fechler N, Tiruye GA, Marcilla R, Antonietti M. Vanadium nitride@N-doped carbon nanocomposites: tuning of pore structure and particle size through salt templating and its influence on supercapacitance in ionic liquid media. *RSC Adv* 2014;4:26981-9. DOI
119. Shalom M, Molinari V, Esposito D, et al. Sponge-like nickel and nickel nitride structures for catalytic applications. *Adv Mater* 2014;26:1272-6. DOI
120. Choi D, Kumta PN. Synthesis, structure, and electrochemical characterization of nanocrystalline tantalum and tungsten nitrides. *J Am Chem Soc* 2007;90:3113-20.
121. Gregoryanz E, Sanloup C, Somayazulu M, et al. Synthesis and characterization of a binary noble metal nitride. *Nat Mater* 2004;3:294-7. DOI
122. Zerr A, Miehe G, Serghiou G, et al. Synthesis of cubic silicon nitride. *Nature* 1999;400:340-2. DOI
123. Li Z, Gordon RG, Pallem V, Li H, Shenai DV. Direct-liquid-injection chemical vapor deposition of nickel nitride films and their reduction to nickel films. *Chem Mater* 2010;22:3060-6. DOI
124. Aguas MM, Nartowski AP, Parkin I, MacKenzie MJ, Craven A. Chromium nitrides (CrN, Cr_2N) from solid state metathesis reactions: effects of dilution and nitriding reagent. *J Mater Chem* 1998;8:1875-80. DOI
125. Xu F, Xie Y, Zhang X, Zhang S, Shi L. A benzene-thermal metathesis route to pure metastable rocksalt GaN. *New J Chem* 2003;27:565-7. DOI
126. Jackson AW, Hector AL. A nonoxidic sol-gel route to titanium nitride and carbonitride films by primary aminecondensation. *J Mater Chem* 2007;17:1016-22. DOI
127. Veith GM, Lupini AR, Baggetto L, et al. Evidence for the formation of nitrogen-rich platinum and palladium nitride nanoparticles. *Chem Mater* 2013;25:4936-45. DOI
128. Guo R, Zhang K, Liu Y, et al. Hydrothermal synthesis of palladium nitrides as robust multifunctional electrocatalysts for fuel cells. *J Mater Chem A* 2021;9:6196-204. DOI
129. Sun L, Liu B. Mesoporous PdN alloy nanocubes for efficient electrochemical nitrate reduction to ammonia. *Adv Mater* ;2022:2207305. DOI
130. Vaughn Ii DD, Araujo J, Meduri P, et al. Solution synthesis of Cu_3PdN nanocrystals as ternary metal nitride electrocatalysts for the oxygen reduction reaction. *Chem Mater* 2014;26:6226-32. DOI
131. Shao M. Palladium-based electrocatalysts for hydrogen oxidation and oxygen reduction reactions. *J Power Sources* 2011;196:2433-44. DOI
132. Wu J, Yang H. Platinum-based oxygen reduction electrocatalysts. *Accounts Chem Res* 2013;46:1848-57. DOI
133. Xie Y, Cai J, Wu Y, et al. Boosting water dissociation kinetics on Pt-Ni nanowires by N-induced orbital tuning. *Adv Mater* 2019;31:1807780. DOI
134. Lee S, Jung JY, Jang I, et al. Anion constructor for atomic-scale engineering of antiperovskite crystals for electrochemical reactions. *Adv Funct Mater* 2021;31:2009241. DOI
135. Yang H, Li S, Feng F, et al. Palladium nanoparticles with surface enrichment of palladium oxide species immobilized on the aniline-functionalized graphene as an advanced electrocatalyst of ethanol oxidation. *ACS Sustain Chem Eng* 2019;7:14621-8. DOI
136. Guerrero-Ortega LPA, Ramírez-Meneses E, Cabrera-Sierra R, et al. Pd and Pd@PdO core–shell nanoparticles supported on Vulcan carbon XC-72R: comparison of electroactivity for methanol electro-oxidation reaction. *J Mater Sci* 2019;54:13694-714. DOI
137. Xiao JW, Fan SX, Wang F, et al. Porous Pd nanoparticles with high photothermal conversion efficiency for efficient ablation of cancer cells. *Nanoscale* 2014;6:4345-51. DOI
138. Ren M, Kang Y, He W, et al. Origin of performance degradation of palladium-based direct formic acid fuel cells. *Appl Catal B* 2011;104:49-53. DOI
139. Oh S-H, Hoflund GB. Low-temperature catalytic carbon monoxide oxidation over hydrous and anhydrous palladium oxide powders. *J Catal* 2007;245:35-44. DOI
140. Hu W, Li GX, Chen JJ, et al. Enhanced catalytic performance of a PdO catalyst prepared via a two-step method of in situ reduction-oxidation. *Chem Commun* 2017;53:6160-3. DOI
141. Jiang B, Song S, Wang J, et al. Nitrogen-doped graphene supported Pd@PdO core-shell clusters for C-C coupling reactions. *Nano Res* 2014;7:1280-90. DOI
142. Wang TJ, Li FM, Huang H, et al. Porous Pd-PdO nanotubes for methanol electrooxidation. *Adv Funct Mater* 2020;30:2000534. DOI
143. Lin R, Luo MF, Xin Q, Sun GQ. The mechanism studies of ethanol oxidation on PdO catalysts by TPSR techniques. *Catal Lett* 2004;93:139-44. DOI
144. Kibis LS, Stadnichenko AI, Koscheev SV, Zaikovskii VI, Boronin AI. Highly oxidized palladium nanoparticles comprising Pd^{4+} species: spectroscopic and structural aspects, thermal stability, and reactivity. *J Phys Chem C* 2012;116:19342-8. DOI
145. Kuriganova AB, Faddeev NA, Leontyev IN, et al. New electrochemical approach for the synthesis of Pd-PdO/C electrocatalyst and application to formic acid electrooxidation. *ChemistrySelect* 2019;4:8390-3. DOI

146. Yao S, Li G, Liu C, Xing W. Enhanced catalytic performance of carbon supported palladium nanoparticles by in-situ synthesis for formic acid electrooxidation. *J Power Sources* 2015;284:355-60. DOI
147. Yang F, Wang C, Dong S, et al. Plasma synthesis of Pd/PdO supported on porous graphene as electrocatalyst for methanol oxidation. *Mater Lett* 2016;174:192-6. DOI
148. Gao N, Ma R, Wang X, et al. Activating the Pd-based catalysts via tailoring reaction interface towards formic acid dehydrogenation. *Int J Hydrogen Energy* 2020;45:17575-82. DOI
149. Lv Q, Meng Q, Liu W, et al. Pd-PdO interface as active site for HCOOH selective dehydrogenation at ambient condition. *J Phys Chem C* 2018;122:2081-8. DOI
150. Lv J, Wu S, Tian Z, et al. Construction of PdO-Pd interfaces assisted by laser irradiation for enhanced electrocatalytic N_2 reduction reaction. *J Mater Chem A* 2019;7:12627-34. DOI
151. Zhou Y, Zhu X, Zhang B, et al. High performance formic acid fuel cell benefits from Pd-PdO catalyst supported by ordered mesoporous carbon. *Int J Hydrogen Energy* 2020;45:29235-45. DOI
152. Ding K, Li Y, Zhao Y, et al. Dry-grinding synthesized multi-walled carbon nanotubes supported PdO catalyst for ethanol oxidation reaction. *Electrochim Acta* 2014;149:186-92. DOI
153. Chen C, Yeh YH, Cargnello M, et al. Methane oxidation on Pd@ZrO_2/Si-Al_2O_3 is enhanced by surface reduction of ZrO_2. *ACS Catal* 2014;4:3902-9. DOI
154. Ding K, Qu R, Han J, et al. Unexpected facilitation of the pyrolysis products of potassium ferrocyanide to the electrocatalytic activity of a PdO based palladium iron composite catalyst towards ethanol oxidation reaction (EOR). *Int J Hydrogen Energy* 2021;46:633-44. DOI
155. Li HC, Zhang YJ, Hu X, et al. Metal-organic framework templated Pd@PdO-Co_3O_4 nanocubes as an efficient bifunctional oxygen electrocatalyst. *Adv Energy Mater* 2018;8:1702734. DOI
156. Cargnello M, Jaén JJD, Garrido JCH, et al. Exceptional activity for methane combustion over modular Pd@CeO_2 subunits on functionalized Al_2O_3. *Science* 2012;337:713-7. DOI
157. Liu J, Luo Z, Li J, et al. Graphene-supported palladium phosphide PdP_2 nanocrystals for ethanol electrooxidation. *Appl Catal B* 2019;242:258-66. DOI
158. Zou X, Rui Z, Ji H. Core-shell NiO@PdO nanoparticles supported on alumina as an advanced catalyst for methane oxidation. *ACS Catal* 2017;7:1615-25. DOI
159. Alyani M, Smith KJ. Kinetic analysis of the inhibition of CH_4 oxidation by H_2O on PdO/Al_2O_3 and CeO_2/PdO/Al_2O_3 catalysts. *Ind Eng Chem Res* 2016;55:8309-18. DOI
160. Du L, Qian K, Zhu X, et al. Interface engineering of palladium and zinc oxide nanorods with strong metal-support interactions for enhanced hydrogen production from base-free formaldehyde solution. *J Mater Chem A* 2019;7:8855-64. DOI
161. Meher S, Rana RK. A rational design of a Pd-based catalyst with a metal-metal oxide interface influencing molecular oxygen in the aerobic oxidation of alcohols. *Green Chem* 2019;21:2494-503. DOI
162. Narayanaru S, Anilkumar GM, Ito M, Tamaki T, Yamaguchi T. An enhanced electrochemical CO_2 reduction reaction on the SnO_x-PdO surface of SnPd nanoparticles decorated on N-doped carbon fibers. *Catal Sci Technol* 2021;11:143-51. DOI
163. Li Y, Kidkhunthod P, Zhou Y, Wang X, Lee JM. Dense heterointerfaces and unsaturated coordination synergistically accelerate electrocatalysis in Pt/Pt_5P_2 porous nanocages. *Adv Funct Mater* 2022;32:2205985. DOI
164. Zhang J, Xu Y, Zhang B. Facile synthesis of 3D Pd-P nanoparticle networks with enhanced electrocatalytic performance towards formic acid electrooxidation. *Chem Commun* 2014;50:13451-3. DOI
165. Lv H, Teng Y, Wang Y, Xu D, Liu B. Highly branched and defect-rich PdP nanosheets for ethanol oxidation electrocatalysis. *Chem Commun* 2020;56:15667-70. DOI
166. Yang H, Yu Z, Li S, et al. Ultrafine palladium-gold-phosphorus ternary alloyed nanoparticles anchored on ionic liquids-noncovalently functionalized carbon nanotubes with excellent electrocatalytic property for ethanol oxidation reaction in alkaline media. *J Catal* 2017;353:256-64. DOI
167. Xie H, Geng Q, Zhu X, et al. PdP_2 nanoparticles–reduced graphene oxide for electrocatalytic N_2 conversion to NH_3 under ambient conditions. *J Mater Chem A* 2019;7:24760-4. DOI
168. Zhao M, Abe K, Yamaura SI, Yamamoto Y, Asao N. Fabrication of Pd-Ni-P metallic glass nanoparticles and their application as highly durable catalysts in methanol electro-oxidation. *Chem Mater* 2014;26:1056-61. DOI
169. Chen L, Lu L, Zhu H, et al. Improved ethanol electrooxidation performance by shortening Pd-Ni active site distance in Pd-Ni-P nanocatalysts. *Nat Commun* 2017;8:14136. DOI
170. Zhang K, Wang C, Bin D, et al. Fabrication of Pd/P nanoparticle networks with high activity for methanol oxidation. *Catal Sci Technol* 2016;6:6441-7. DOI
171. Cheng L, Zhang Z, Niu W, Xu G, Zhu L. Carbon-supported Pd nanocatalyst modified by non-metal phosphorus for the oxygen reduction reaction. *J Power Sources* 2008;182:91-4. DOI
172. Tianou H, Wang W, Yang X, et al. Inflating hollow nanocrystals through a repeated Kirkendall cavitation process. *Nat Commun* 2017;8:1261. DOI
173. Yang H, Li S, Jin R, et al. Surface engineering of phosphorus low-doping palladium nanoalloys anchored on the three-dimensional nitrogen-doped graphene for enhancing ethanol electroxidation. *Chem Eng J* 2020;389:124487. DOI
174. Luo F, Zhang Q, Yu X, et al. Palladium phosphide as a stable and efficient electrocatalyst for overall water splitting. *Angew Chem Int*

Ed 2018;57:14862-7. DOI
175. Furukawa S, Matsunami Y, Hamada I, et al. Remarkable enhancement in hydrogenation ability by phosphidation of ruthenium: specific surface structure having unique Ru ensembles. *ACS Catal* 2018;8:8177-81. DOI
176. Pu Z, Zhao J, Amiinu IS, et al. A universal synthesis strategy for P-rich noble metal diphosphide-based electrocatalysts for the hydrogen evolution reaction. *Energ Environ Sci* 2019;12:952-7. DOI
177. Yu J, Wu X, Zhang H, et al. Core effect on the performance of N/P codoped carbon encapsulating noble-metal phosphide nanostructures for hydrogen evolution reaction. *ACS Appl Energy Mater* 2019;2:2645-53. DOI
178. Yang G, Chen Y, Zhou Y, Tang Y, Lu T. Preparation of carbon supported Pd-P catalyst with high content of element phosphorus and its electrocatalytic performance for formic acid oxidation. *Electrochem Commun* 2010;12:492-5. DOI
179. Poon KC, Tan DCL, Vo TDT, et al. Newly developed stepwise electroless deposition enables a remarkably facile synthesis of highly active and stable amorphous Pd nanoparticle electrocatalysts for oxygen reduction reaction. *J Am Chem Soc* 2014;136:5217-20. DOI
180. Wang R, Ma Y, Wang H, Key J, Ji S. Gas-liquid interface-mediated room-temperature synthesis of "clean" PdNiP alloy nanoparticle networks with high catalytic activity for ethanol oxidation. *Chem Commun* 2014;50:12877-9. DOI
181. Wang Y, Shi FF, Yang YY, Cai WB. Carbon supported Pd-Ni-P nanoalloy as an efficient catalyst for ethanol electro-oxidation in alkaline media. *J Power Sources* 2013;243:369-73. DOI
182. Lv H, Sun L, Xu D, Ma Y, Liu B. When ternary PdCuP alloys meet ultrathin nanowires: synergic boosting of catalytic performance in ethanol electrooxidation. *Appl Catal B* 2019;253:271-7. DOI
183. Jiang R, Tran DT, McClure JP, Chu D. A class of (Pd-Ni-P) electrocatalysts for the ethanol oxidation reaction in alkaline media. *ACS Catal* 2014;4:2577-86. DOI
184. Wang H, Yang D, Liu S, et al. Metal-nonmetal one-dimensional electrocatalyst: AuPdP nanowires for ambient nitrogen reduction to ammonia. *ACS Sustain Chem Eng* 2019;7:15772-7. DOI
185. Li C, Xu Y, Deng K, et al. Metal-nonmetal nanoarchitectures: quaternary PtPdNiP mesoporous nanospheres for enhanced oxygen reduction electrocatalysis. *J Mater Chem A* 2019;7:3910-6. DOI
186. Xu Y, Ren K, Ren T, et al. Phosphorus-triggered modification of the electronic structure and surface properties of Pd_4S nanowires for robust hydrogen evolution electrocatalysis. *J Mater Chem A* 2020;8:19873-8. DOI
187. Yin S, Wang Z, Zhang H, et al. Enhancing hydrogen evolution activity of triangular PtPdCu nanodarts by phosphorus incorporation. *Chem Eng J* 2020;399:125810. DOI
188. Shreyanka S, Theerthagiri J, Lee SJ, Yu Y, Choi MY. Multiscale design of 3D metal-organic frameworks (M-BTC, M: Cu, Co, Ni) via PLAL enabling bifunctional electrocatalysts for robust overall water splitting. *Chem Eng J* 2022;446:137045. DOI
189. Zhang L, Lu D, Chen Y, Tang Y, Lu T. Facile synthesis of Pd-Co-P ternary alloy network nanostructures and their enhanced electrocatalytic activity towards hydrazine oxidation. *J Mater Chem A* 2014;2:1252-6. DOI
190. Yin PF, Zhou M, Chen J, et al. Synthesis of palladium-based crystalline@amorphous core-shell nanoplates for highly efficient ethanol oxidation. *Adv Mater* 2020;32:2000482. DOI
191. Broadbent HS, Slaugh LH, Jarvis NL. Rhenium sulfides as liquid-phase hydrogenation catalysts. a comparison with molybdenum sulfide and cobalt polysulfide. *J Am Chem Soc* 1954;76:1519-23. DOI
192. Yoon D, Seo B, Lee J, et al. Facet-controlled hollow Rh_2S_3 hexagonal nanoprisms as highly active and structurally robust catalysts toward hydrogen evolution reaction. *Energy Environ Sci* 2016;9:850-6. DOI
193. Singh VV, Kumar U, Tripathi SN, Singh AK. Shape dependent catalytic activity of nanoflowers and nanospheres of Pd_4S generated via one pot synthesis and grafted on graphene oxide for Suzuki coupling. *Dalton Trans* 2014;43:12555-63. DOI
194. Xu W, Ni J, Zhang Q, et al. Tailoring supported palladium sulfide catalysts through H_2-assisted sulfidation with H_2S. *J Mater Chem A* 2013:1. DOI
195. O'Brien CP, Howard BH, Miller JB, Morreale BD, Gellman A J. Inhibition of hydrogen transport through Pd and $Pd_{47}Cu_{53}$ membranes by H_2S at 350 °C. *J Membr Sci* 2010;349:380-4. DOI
196. Kabe T, Qian W, Hirai Y, Li L, Ishihara A. Hydrodesulfurization and hydrogenation reactions on noble metal catalysts: I. Elucidation of the behavior of sulfur on alumina-supported platinum and palladium using the ^{35}S radioisotope tracer method. *J Catal* 2000;190:191-8. DOI
197. Mori A, Mizusaki T, Kawase M, et al. Novel palladium-on-carbon/diphenyl sulfide complex for chemoselective hydrogenation: preparation, characterization, and application. *Adv Synth Catal* 2008;350:406-10. DOI
198. Schultz M, Matijević E. Preparation and properties of nanosized PdS dispersions for electrolytic plating. *Colloids Surf A* 1998;131:173-9. DOI
199. O'Brien P, Waters J. Deposition of Ni and Pd sulfide thin films via aerosol-assisted CVD. *Chem Vap Deposition* 2006;12:620-6. DOI
200. Radha B, Kulkarni GU. Patterned synthesis of Pd_4S: chemically robust electrodes and conducting etch masks. *Adv Funct Mater* 2010;20:879-84. DOI
201. Greeley J, Stephens IEL, Bondarenko AS, et al. Alloys of platinum and early transition metals as oxygen reduction electrocatalysts. *Nat Chem* 2009;1:552-6. DOI
202. Du C, Li P, Yang F, et al. Monodisperse palladium sulfide as efficient electrocatalyst for oxygen reduction reaction. *ACS Appl Mater Interf* 2018;10:753-61. DOI
203. Ma L, Yuan S, Jiang T, et al. Pd_4S/SiO_2: a sulfur-tolerant palladium catalyst for catalytic complete oxidation of methane. *Catalysts* 2019;9:410. DOI

204. Yang J, Yan H, Wang X, et al. Roles of cocatalysts in Pt-PdS/CdS with exceptionally high quantum efficiency for photocatalytic hydrogen production. *J Catal* 2012;290:151-7. DOI
205. McCue AJ, Guerrero-Ruiz A, Rodríguez-Ramos I, Anderson JA. Palladium sulphide-A highly selective catalyst for the gas phase hydrogenation of alkynes to alkenes. *J Catal* 2016;340:10-6. DOI
206. Li X, Yang G, Li S, et al. Novel dual co-catalysts decorated Au@HCS@PdS hybrids with spatially separated charge carriers and enhanced photocatalytic hydrogen evolution activity. *Chem Eng J* 2020;379:122350. DOI
207. McCue AJ, Guerrero-Ruiz A, Ramirez-Barria C, Rodríguez-Ramos I, Anderson JA. Selective hydrogenation of mixed alkyne/alkene streams at elevated pressure over a palladium sulfide catalyst. *J Catal* 2017;355:40-52. DOI
208. Zubkov A, Fujino T, Sato N, Yamada K. Enthalpies of formation of the palladium sulphides. *J Chem Thermodyn* 1998;30:571-81. DOI
209. Zhang Q, Feng F, Su C, et al. Preparation of supported core-shell structured Pd@Pd_xS_y/C catalysts for use in selective reductive alkylation reaction. *RSC Adv* 2015;5:66278-85. DOI
210. Zhang Q, Xu W, Li X, et al. Catalytic hydrogenation of sulfur-containing nitrobenzene over Pd/C catalysts: In situ sulfidation of Pd/C for the preparation of PdxSy catalysts. *Appl Catal A* 2015;497:17-21. DOI
211. Liu Y, McCue AJ, Feng J, et al. Evolution of palladium sulfide phases during thermal treatments and consequences for acetylene hydrogenation. *J Catal* 2018;364:204-15. DOI
212. Huang Y, Seo K D, Park DS, Park H, Shim YB. Hydrogen evolution and oxygen reduction reactions in acidic media catalyzed by Pd_4 S decorated N/S doped carbon derived from Pd coordination polymer. *Small* 2021;17:e2007511. DOI
213. Wang Y, Xu K, Zhu Z, et al. Sulfurization-induced partially amorphous palladium sulfide nanosheets for highly efficient electrochemical hydrogen evolution. *Chem Commun* 2021;57:1368-71. DOI
214. Novakova EK, McLaughlin L, Burch R, et al. Palladium-catalyzed liquid-phase hydrogenation/hydrogenolysis of disulfides. *J Catal* 2007;249:93-101. DOI
215. Bach LG, Thi MLN, Bui QB, Nhac-Vu HT. Palladium sulfide nanoparticles attached MoS_2/nitrogen-doped graphene heterostructures for efficient oxygen reduction reaction. *Synth Met* 2019;254:172-9. DOI
216. Wang F, Shifa TA, Zhan X, et al. Recent advances in transition-metal dichalcogenide based nanomaterials for water splitting. *Nanoscale* 2015;7:19764-88. DOI
217. Lv H, Sun L, Xu D, Liu B. Ternary metal-metalloid-nonmetal alloy nanowires: a novel electrocatalyst for highly efficient ethanol oxidation electrocatalysis. *Sci Bull* 2020;65:1823-31. DOI
218. Lv H, Xu D, Sun L, et al. Ternary palladium-boron-phosphorus alloy mesoporous nanospheres for highly efficient electrocatalysis. *ACS Nano* 2019;13:12052-61. DOI
219. Yin S, Xu Y, Liu S, et al. Binary nonmetal S and P-co-doping into mesoporous PtPd nanocages boosts oxygen reduction electrocatalysis. *Nanoscale* 2020;12:14863-9. DOI
220. Xu Y, Yu S, Ren T, et al. A quaternary metal-metalloid-nonmetal electrocatalyst: B, P-co-doping into PdRu nanospine assemblies boosts the electrocatalytic capability toward formic acid oxidation. *J Mater Chem A* 2020;8:2424-9. DOI
221. Zhang G, Wang A, Niu L, et al. Interfacial engineering to construct antioxidative $Pd_4S/Pd_3P_{0.95}$ heterostructure for robust hydrogen production at high current density. *Adv Energy Mater* 2022;12:2103511. DOI
222. Zhang W, Lin W, Ren J, Zheng N, Wu B. Electrochemical reduction of nitrogen to ammonia by Pd-S-Mo nanosheets on a hydrophobic hierarchical graphene support. *ChemElectroChem* 2022;9:e202100052. DOI
223. Xu Y, Wang M, Yu S, et al. Electronic structure control over Pd nanorods by B, P-co-doping enables enhanced electrocatalytic performance. *Chem Eng J* 2021;421:127751. DOI
224. Guo X, Chen Z, Huang Y, et al. Mesoporous palladium-boron-sulfur alloy nanospheres for efficient hydrogen evolution. *Inorg Chem* 2021;60:4380-4. DOI